frontiers | Frontiers in Earth Science
ORIGINAL RESEARCH
published: 03 May 2022
doi: 10.3389/feart.2021.825852

Prolonged Late Mesoproterozoic to Late Triassic Tectonic Evolution of the Major Paleo-Asian Ocean in the Beishan Orogen (NW China) in the Southern Altaids

Qigui Mao[1,2]*, Wenjiao Xiao[1,3,4,5]*, Hao Wang[1]*, Songjian Ao[3,4,5], Brian F. Windley[6], Dongfang Song[3,4], Miao Sang[1], Zhou Tan[1], Rui Li[1] and Meng Wang[1,7]

[1]Xinjiang Research Center for Mineral Resources, Xinjiang Institute of Ecology and Geography, Chinese Academy of Sciences, Urumqi, China, [2]Redrock Mining CO., Ltd., Hami, China, [3]State Key Laboratory of Lithospheric Evolution, Institute of Geology and Geophysics, Chinese Academy of Sciences, Beijing, China, [4]College of Earth and Planetary Sciences, University of Chinese Academy of Sciences, Beijing, China, [5]China-Pakistan Joint Research Center on Earth Sciences, Chinese Academy of Sciences, Beijing, China, [6]School of Geography, Geology and the Environment, University of Leicester, Leicester, United Kingdom, [7]College of Resource and Environment Sciences, Xinjiang University, Urumqi, China

OPEN ACCESS

Edited by:
Xiubin Lin,
Zhejiang University, China

Reviewed by:
Yongjiang Liu,
Ocean University of China, China
Jian-Bo Zhou,
Jilin University, China

***Correspondence:**
Qigui Mao
qg_mao@sina.cn
Wenjiao Xiao
wj-xiao@mail.iggcas.ac.cn
Hao Wang
wanghao@ms.xjb.ac.cn

Specialty section:
This article was submitted to Structural Geology and Tectonics, a section of the journal Frontiers in Earth Science

Received: 30 November 2021
Accepted: 10 December 2021
Published: 03 May 2022

Citation:
Mao Q, Xiao W, Wang H, Ao S, Windley BF, Song D, Sang M, Tan Z, Li R and Wang M (2022) Prolonged Late Mesoproterozoic to Late Triassic Tectonic Evolution of the Major Paleo-Asian Ocean in the Beishan Orogen (NW China) in the Southern Altaids. Front. Earth Sci. 9:825852. doi: 10.3389/feart.2021.825852

The accretionary processes and the continental growth of the Altaids are still controversial. The Beishan orogen is situated in the southernmost Altaids and is an ideal tectonic site to address these issues. In this study, we report the results of new field-based lithological mapping and structural analysis on the Huaniushan complex in the Beishan orogen, which is composed of blocks of serpentinized ultramafic, gabbro, basalt, chert, limestone, and other rocks within a strongly deformed and cleaved matrix of sandstone and schist. Our new zircon U-Pb date reveal that a gabbro block formed at 504 ± 3 Ma. Our geochemical and isotopic data of gabbroic and basaltic blocks show that they are relics of the Mid-Ocean-Ridge (MORB)-type and Ocean-Island-Basalt (OIB)-type oceanic lithosphere, with high values of $\varepsilon_{Nd}(t)$ (+4.3–+14.5) and $\varepsilon_{Hf}(t)$ (+8.07–+17.74). The maximum depositional ages (MDAs) of two sandstone blocks were dated at 309 ± 5 Ma and 502 ± 11 Ma, respectively. U-Pb ages and Hf isotopes of detrital zircons from the matrix sandstones indicate that they were derived only from the Shuangyingshan–Huaniushan arc to the north. Accordingly, the Huaniushan complex was part of the Liuyuan accretionary complex that fringed the Huaniushan arc, and, therefore, formed by the northward subduction of the Liuyuan oceanic plate. Combined with the basalt yields zircon U-Pb age of 1,071 ± 5 Ma, we concluded that the Huaniushan complex has an age of 1,071 Ma to 309 Ma. Furthermore, the oceanic blocks and sedimentary matrix of the Liuyuan accretionary complex have an age of 1,071–270 Ma and 920–234 Ma, respectively, suggesting that the Liuyuan Ocean was still open at ca. 234 Ma. Thus, the studies reveal that the Liuyuan Ocean, a major branch of the Paleo-Asian Ocean, may have experienced a prolonged tectonic history, starting in the late Mesoproterozoic (1,071 Ma) and terminating later than the late Triassic (234 Ma), with a long subduction and development of a series of seamounts and/or plateaus emplaced into the Liuyuan accretionary complex.

Keywords: late mesoproterozoic–late triassic, Huaniushan complex, Liuyuan accretionary complex, southern Beishan, altaids

INTRODUCTION

The Altaids or the southern Central Asian Orogenic Belt was a most critical site of juvenile crustal growth, lying among the European craton to the west, the Siberian craton to the north, and the Tarim and North China cratons to the south (Kröner et al., 2007; Windley et al., 2007; Schulmann and Paterson, 2011; Wilhem et al., 2012; Xiao et al., 2013; Safonova and Santosh, 2014; Xiao et al., 2018) (**Figure 1A**). It experienced long-lived accretion of island arcs, continental arcs, seamounts, microcontinents, and accretionary complexes (Coleman, 1989; Allen et al., 1995; Dobretsov et al., 1995; Buchan et al., 2002; Bazhenov et al., 2003; Kröner et al., 2007; Windley et al., 2007; Xiao et al., 2018; Liu et al., 2021). The Altaids is generally regarded as a result of the final formation of the Kazakhstan and Tuva–Mongol oroclines, accompanying the convergence of the

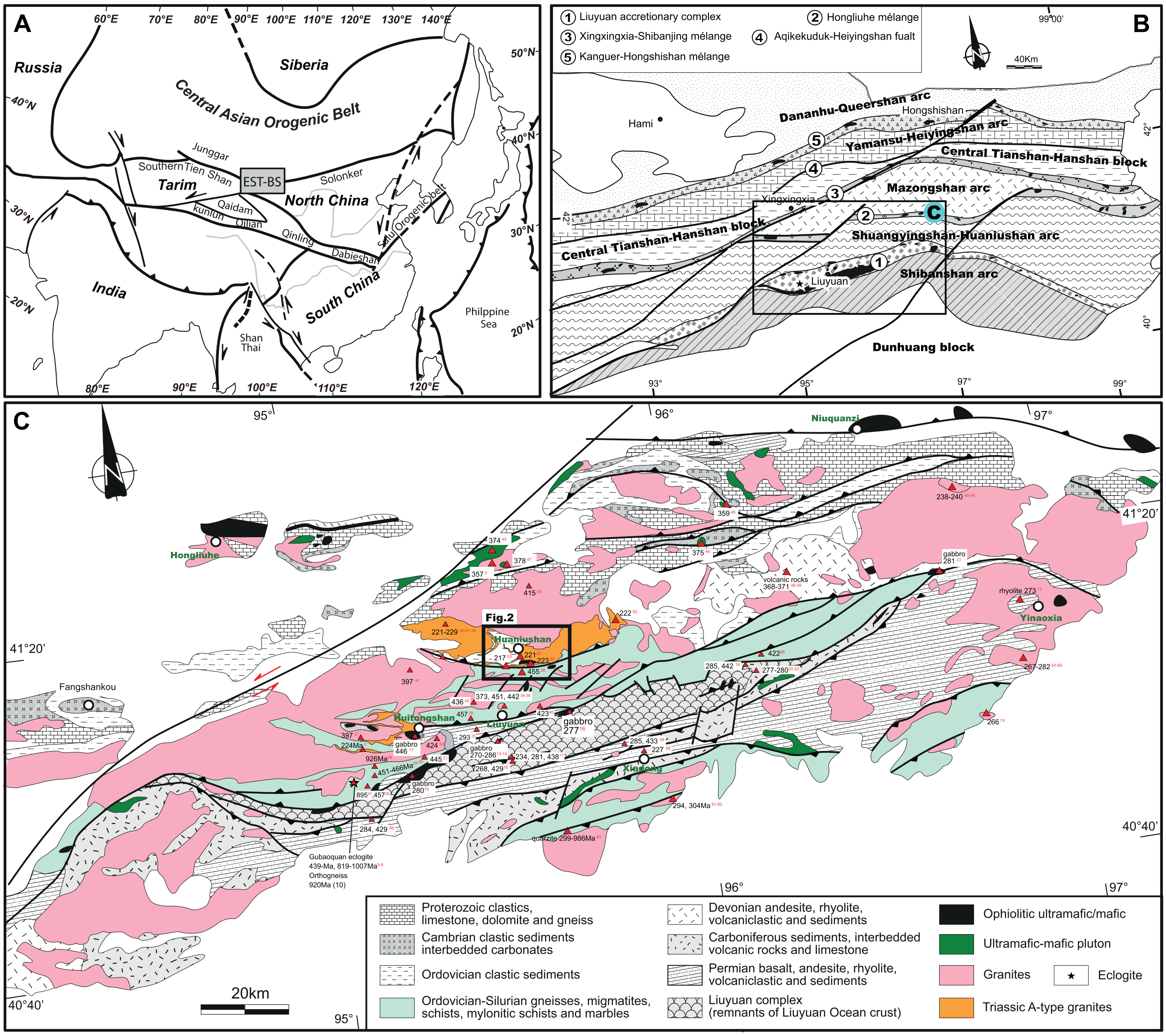

FIGURE 1 | (A) Schematic tectonic map of Central Asia and adjacent regions, showing the tectonic position of the Beishan orogen (Şengör et al., 1993; Xiao et al., 2018) EST-BS, eastern Tianshan-Beishan orogen. **(B)** Tectonic map of the Beishan orogenic belt, showing the position of the Liuyuan accretionary complex in relation to the three main arcs (Xiao et al., 2010). **(C)** Geological map of the Liuyuan accretionary complex and adjacent areas showing the relations with the main stratigraphic units of the Beishan (GSBGMR, 1989; Mao et al., 2012b).

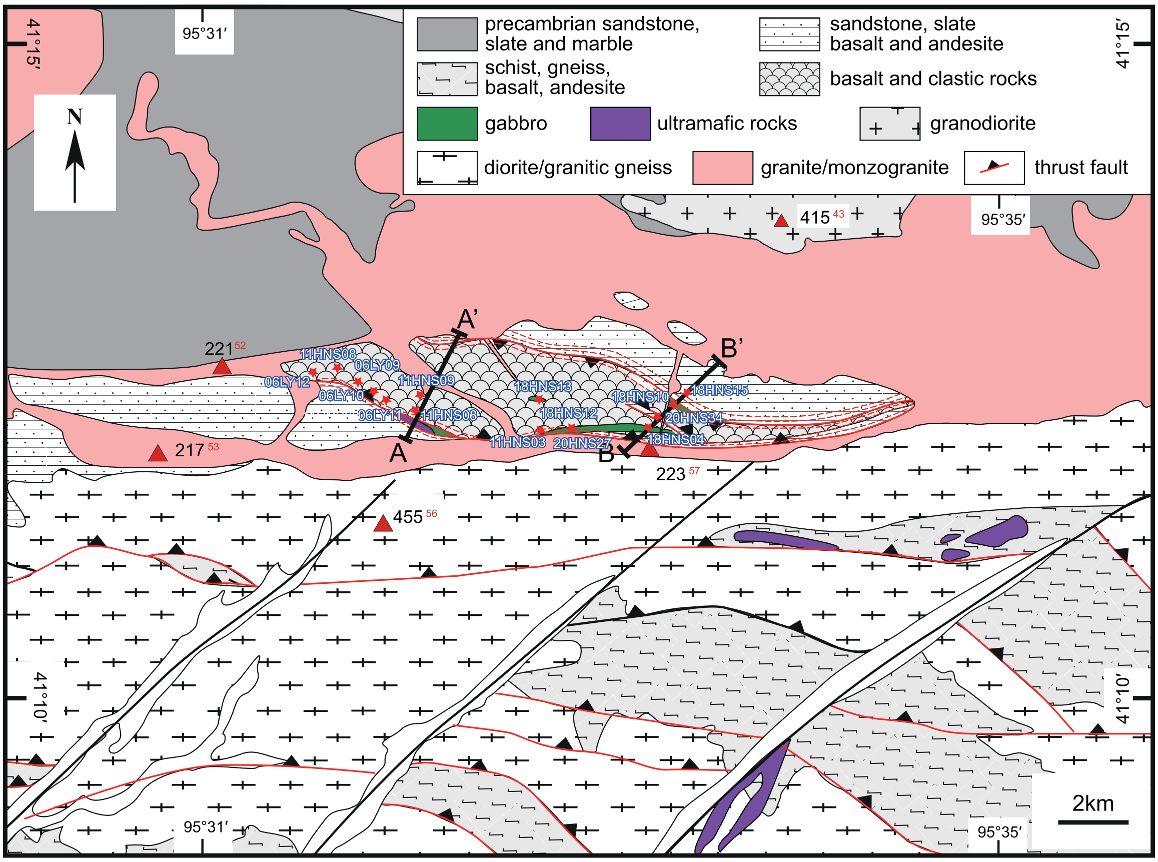

FIGURE 2 | Geological map of the Huaniushan complex in the northern part of the Liuyuan accretionary complex.

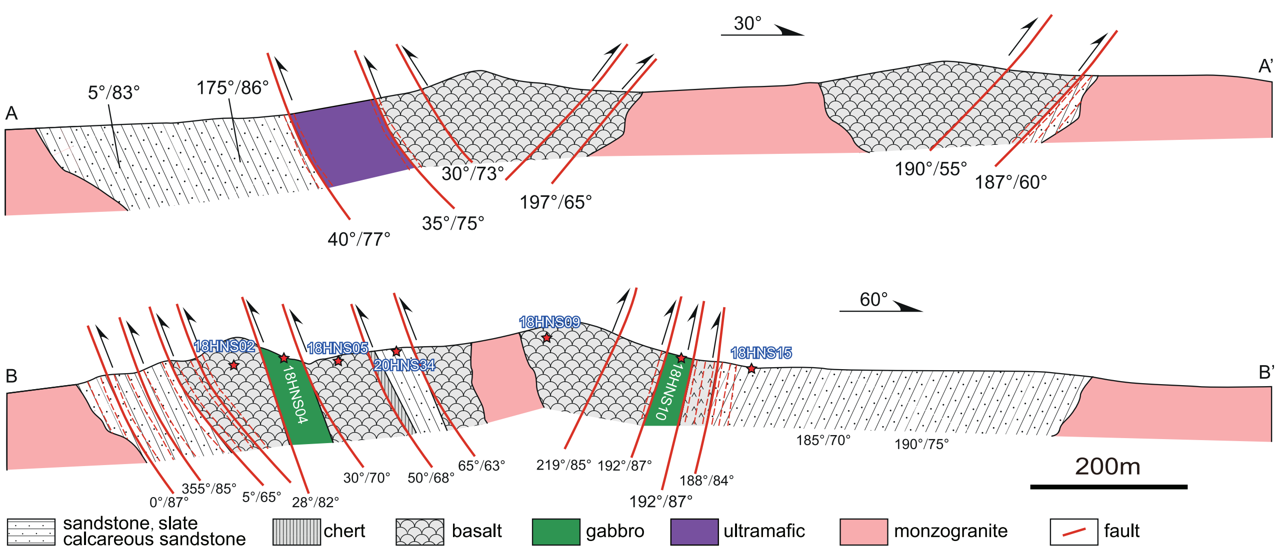

FIGURE 3 | Cross-sections of the Huaniushan complex; **(A)** cross-section (**A-A′**) in the western part; **(C)** cross-section (**B-B′**) in the eastern part.

Tarim and North China cratons along the South Tianshan–Solonker suture zone (Şengör et al., 1993; Xiao et al., 2018). The South Tianshan and Solonker belts are confirmed to be the final suture for the eastern and western segments of the southern Altaids. However, the exact position of the final position of the suture in the middle segment is not clear,

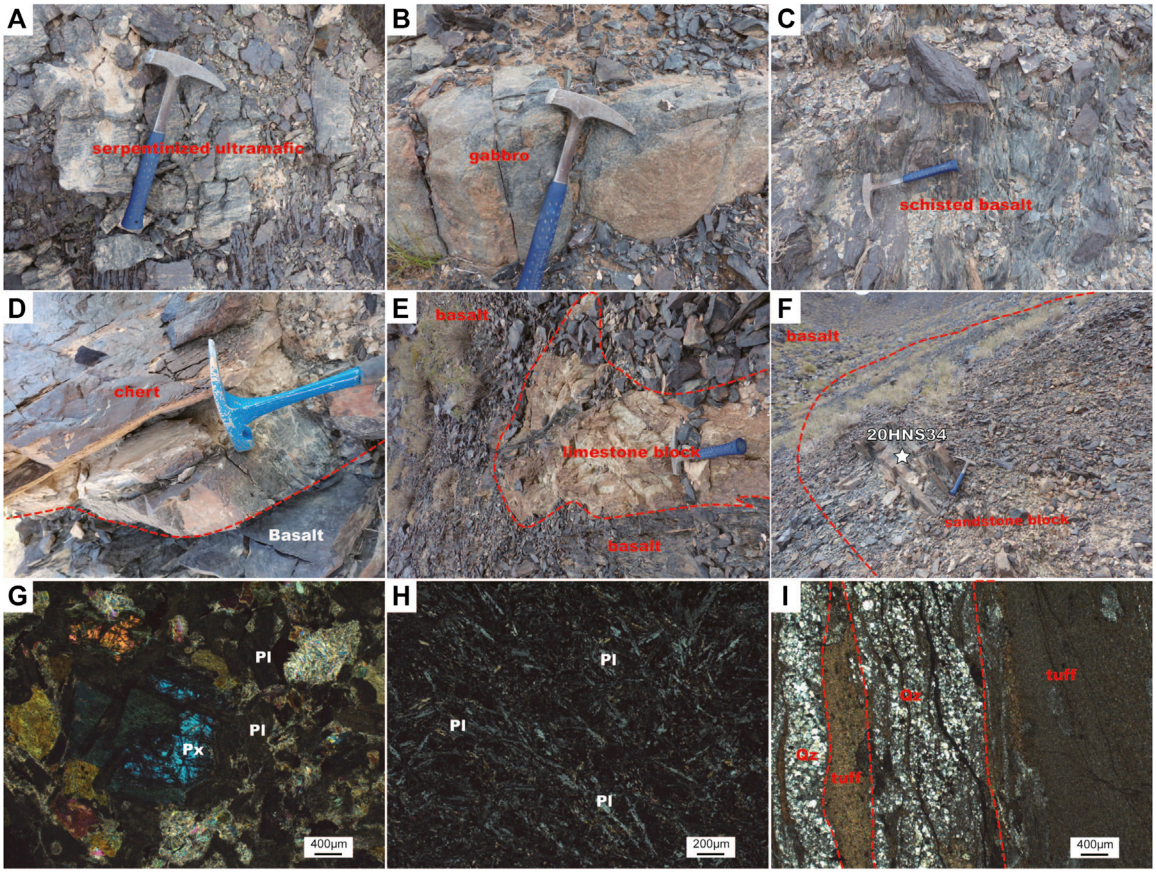

FIGURE 4 | Field photos and microphotos for different rocks of the Huaniushan complex, Beishan. **(A)** Serpentinized ultramafic; **(B)** gabbro; **(C)** schist basalt; **(D)** chert and basalt; **(E)** limestone blocks in basalt; and **(F)** sandstone. **(G–I)** Microphotos of gabbro, basalt, and sandstone. Px, pyroxene; Pl, plagioclase; Qz, quartz.

which hampers our understanding of the accretionary processes of the southern Altaids and continental growth of Central Asia.

The Beishan orogen is the middle segment of the Tianshan–Solonker suture of the southern Altaids (Windley et al., 2007; Domeier and Torsvik, 2014; Xiao et al., 2018; Liu et al., 2021), which is one of the key areas for unraveling the accretionary processes and continental growth of Central Asia (Zuo et al., 1991; Nie et al., 2002a; Xiao et al., 2010; Mao et al., 2012b). It was formed by episodic amalgamation and accretion of continental margin arcs, island arcs, ophiolites, and accretionary wedges. The Liuyuan-Houhongquan mélange complex belt is located at the southern part of Beishan orogen, represents the ancient position of the Paleo-Liuyuan Ocean and one of the final sutures of the Beishan orogen (Windley et al., 2007; Mao et al., 2012b; Domeier and Torsvik, 2014; Xiao et al., 2010), is one of the key areas to constraint the evolution of the Beishan orogen. However, when the ocean opened and the nature of the Liuyuan Ocean and the early-stage tectonic evolution of the Beishan orogen are rarely discussed and debatable (Zuo et al., 1991; Liu and Wang, 1995; Nie et al., 2002a; Xiao et al., 2010; Mao et al., 2012b; Wang et al., 2016; Saktura et al., 2017). In this study, we report our new discovery of Proterozoic to Cambrian ophiolite fragments in the Huaniushan area in the southern Beishan orogen and present new geological, whole-rock geochemical, and Sr-Nd isotopic data for representative mafic rocks to constrain their genesis and reveal the early geodynamic evolution of the southern Altaids.

GEOLOGICAL SETTING

The Beishan Orogen is located in a key tectonic position of the southern Altaids, connecting with the eastern Tianshan suture to the west and the Solonker suture to the east (**Figures 1A,B**). The tectonics of the Beishan collages is characterized by several blocks/arcs separated by several ophiolitic belts which are regarded as suture zones (Zuo et al., 1991; Liu and Wang, 1995; Nie et al., 2002a; Xiao et al., 2010). These major mélange (accretionary complex) belts are the Kanguer-Hongshishan mélange, Xingxingxia-Shibanjin mélange, Hongliuhe mélange and Liuyuan accretionary complex (**Figure 1B**). A detailed description of these fault zones and terranes can be found in related references (Zuo et al., 1991; Liu and Wang, 1995; Nie et al., 2002a; Zuo et al., 2003; Xiao et al., 2010; Mao et al., 2012b). Here, we mainly introduced the regional geology associated with the Shuangyingshan–Huaniushan arc

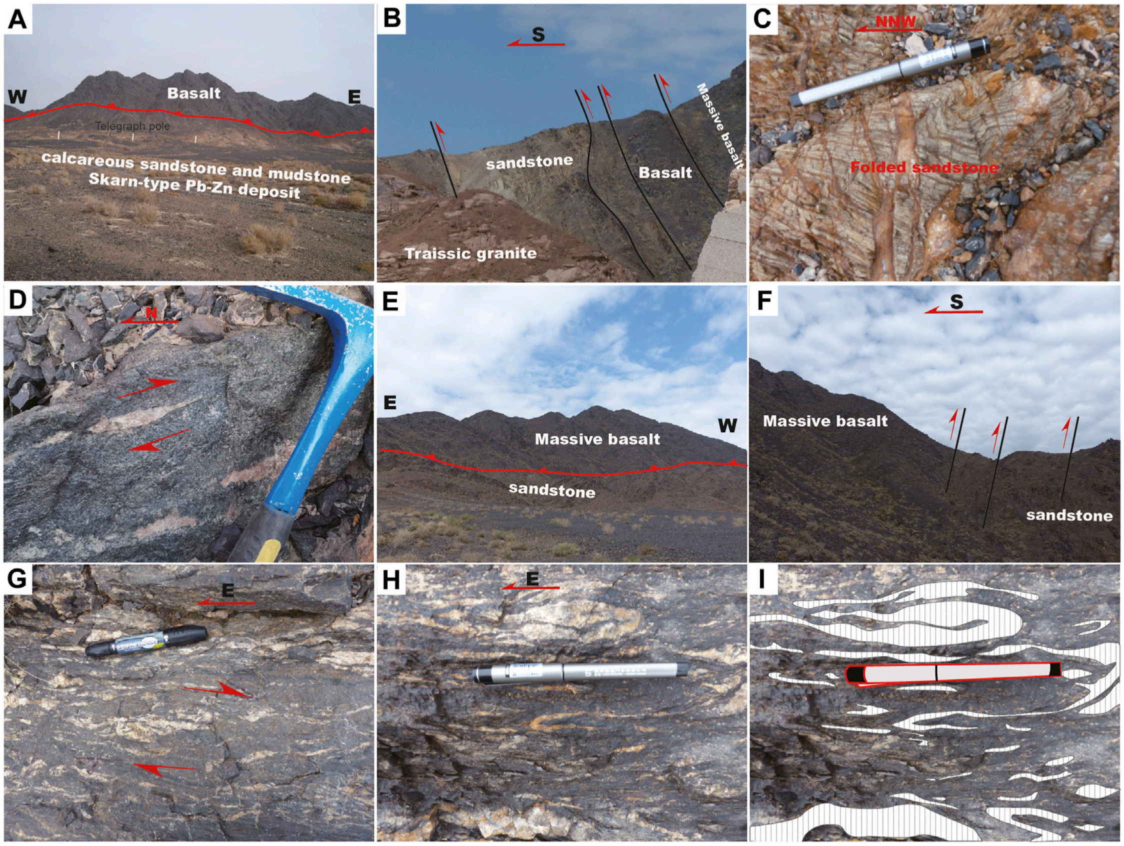

FIGURE 5 | Structural deformation photos for different rocks of the Huaniushan complex, Beishan. **(A)** Huaniushan complex thrust on Huaniushan Formation (O_2*hn*) in the southern part; **(B)** section of the thrust in the southern part; **(C)** folded sediments in the southern part; **(D)** deformed gabbro blocks in the Huaniushan complex; **(F)** Huaniushan complex thrust on sediments in the northern part; **(G)** section of the thrust in the northern part; **(H)** strongly deformed and silicified basalt and suggest the dextral shear; **(I)** strongly deformed, folded, and silicified basalt.

and Liuyuan accretionary complex and Shibanshan arc (**Figures 1B,C**).

The Shuangyingshan–Huaniushan arc is a composite arc, similar to the Japan arc (Xiao et al., 2010; Mao et al., 2012b). The northern part of the Shuangyingshan–Huaniushan arc comprises the Precambrian to Ordovician shelf clastic sediments and carbonates on which the Paleozoic Huaniushan arc was built. The late Proterozoic is characterized by a marine sedimentary layer (Zuo et al., 1991; Nie et al., 2002b; Xiao et al., 2010; Song et al., 2013). The Ordovician–Permian Huaniushan arc developed on the southern margin of the Shuangyingshan block. It comprises Ordovician–Permian calc-alkaline basalts, andesites, rhyolites, tuffs, and volcaniclastic rocks with interlayered clastics and carbonate (GSBGMR, 1989; Zuo et al., 1990; Zuo et al., 1991; Nie et al., 2002a; Xiao et al., 2010; Mao et al., 2012a; 2012b; Guo et al., 2014). A suite of metamorphic rocks is distributed discontinuously on the southern margin of the Huaniushan arc, mainly comprising gneisses, migmatites, schists, and marbles that show greenschist-to eclogite-facies metamorphism (Mei et al., 1998; Mei et al., 1999; Liu et al., 2002; Liu et al., 2011; Qu et al., 2011; Yang et al., 2006). The ages of the complex are not well-constrained; for example, the Ordovician–Silurian ages are mainly designated by regional comparison with the rocks nearby (GSBGMR, 1989; Zuo et al., 1990; Zuo et al., 1991; Nie et al., 2002a). Recently, U-Pb zircon dates reveal that the protolith of the Gubaoquan eclogites has an age of 819–1,007 Ma (Yang et al., 2006; Liu et al., 2011; Qu et al., 2011; Saktura et al., 2017), an augen orthogneiss has a zircon U-Pb age of 920 ± 14 Ma (Saktura et al., 2017), and the sandstone, schist, and mylonite have zircon U-Pb ages ranging from 293 to 457 Ma (Tian and Xiao, 2020; Wang et al., 2016). Different type intrusions are extensive and age of Ordovician to Triassic (**Figure 2**, (Nie et al., 2002a; Nie et al., 2002b; Zhao et al., 2007; Mao et al., 2012a; Li et al., 2012; Wang et al., 2016).

The late Paleozoic Shibanshan arc is located on the northern margin of the Dunhuang block (**Figures 2A,B**), containing low-grade and high-grade metamorphic units. The low-grade unit, on the northern margin of the arc, contains low greenschist facies Devonian–Permian calc-alkaline volcanic rocks, volcaniclastics, tuffs, carbonates, and clastic rocks. The high-grade unit is mainly composed of gneisses, migmatites, schists, mylonitic schists, and marbles, and age of 896–294 Ma (Song et al., 2016; Tian and Xiao, 2020). Abundant granitic intrusions are formed from the

TABLE 1 | Zircon U-Pb ages of gabbros and sediment blocks from the Huaniushan complex in the Beishan orogen, NW China.

Sample no.				Isotopic ratio							Isotopic age (Ma)						Con.
	Th	U	Th/U	$^{207}Pb/^{206}Pb$	2σ	$^{207}Pb/^{235}U$	2σ	$^{206}Pb/^{238}U$	2σ		$^{207}Pb/^{206}Pb$	2σ	$^{207}Pb/^{235}U$	2σ	$^{206}Pb/^{238}U$	2σ	%
Gabbro-20HNS27																	
1	1,161	834	1.39	0.0573	0.0011	0.645	0.017	0.082	0.001		508	44	504	10	508.1	6.2	99
2	782	682	1.15	0.0606	0.0017	0.682	0.018	0.0811	0.001		607	60	527	11	502.5	6.2	105
3	1,680	796	2.11	0.0573	0.0013	0.633	0.016	0.0795	0.0012		499	55	497	10	492.8	7.3	101
4	272	234	1.16	0.0585	0.0024	0.638	0.028	0.0801	0.0013		518	88	501	18	496.9	7.5	101
5	597	549	1.09	0.0579	0.0015	0.627	0.015	0.0799	0.0011		504	58	497	10	495.4	6.4	100
6	2010	690	2.91	0.0603	0.0016	0.688	0.02	0.082	0.001		597	59	531	12	508	6	105
7	188	198	0.95	0.0579	0.0028	0.653	0.035	0.0814	0.0017		500	110	507	21	504	10	101
8	977	577	1.69	0.0615	0.0017	0.69	0.02	0.08063	0.00076		639	61	532	12	500	5	106
9	716	509	1.41	0.059	0.0021	0.657	0.029	0.0821	0.0014		544	78	511	18	509	8	100
10	384	325	1.18	0.058	0.0019	0.648	0.022	0.0814	0.0012		499	74	506	14	505	7	100
11	328	292	1.12	0.0617	0.0033	0.651	0.043	0.081	0.0021		630	120	506	26	502	12	101
12	410	403	1.02	0.0572	0.0022	0.647	0.022	0.0808	0.0013		472	88	505	14	501	8	101
13	345	291	1.19	0.06	0.0027	0.648	0.028	0.0796	0.0014		552	94	505	17	494	8	102
14	494	380	1.30	0.0591	0.003	0.667	0.029	0.0819	0.0017		540	110	517	18	507	10	102
15	127.3	139.1	0.92	0.0608	0.0036	0.695	0.042	0.0829	0.002		570	130	532	25	513	12	104
16	512	444	1.15	0.0584	0.0017	0.656	0.02	0.0815	0.0015		522	61	511	13	505	9	101
17	1,630	860	1.90	0.0577	0.0013	0.657	0.019	0.0822	0.0012		504	49	511	11	510	7	100
18	1,011	774	1.31	0.0602	0.0021	0.668	0.02	0.0824	0.0015		589	74	521	13	510	9	102
19	1,285	816	1.57	0.0581	0.0013	0.667	0.018	0.0829	0.00097		537	46	520	10	513	6	101
20	654	528	1.24	0.0573	0.0017	0.662	0.02	0.0836	0.0012		476	67	515	13	517.6	6.9	99
Sandstone-18HNS15																	
1	122	359	0.34	0.1141	0.0038	4.7946	0.1965	0.3037	0.0070		1866	60	1784	35	1710	34	96
2	203	739	0.28	0.0773	0.0030	1.5225	0.0823	0.1422	0.0042		1,128	66	939	33	857	23	110
3	64	337	0.19	0.0976	0.0033	3.5882	0.1423	0.2661	0.0058		1,589	64	1,547	32	1,521	30	97
4	52	55	0.94	0.0991	0.0065	3.2326	0.2260	0.2365	0.0073		1,609	131	1,465	54	1,368	38	107
5	56	202	0.28	0.0785	0.0039	1.8233	0.0953	0.1685	0.0038		1,161	99	1,054	34	1,004	21	105
6	100	100	1.00	0.1158	0.0056	4.9713	0.2719	0.3106	0.0065		1892	88	1814	46	1744	32	96
7	317	472	0.67	0.0804	0.0034	2.1790	0.1002	0.1966	0.0042		1,206	82	1,174	32	1,157	23	102
8	151	166	0.91	0.1660	0.0061	11.1287	0.4211	0.4863	0.0091		2,518	63	2,534	35	2,555	39	101
9	169	197	0.86	0.1111	0.0041	4.2929	0.1606	0.2803	0.0049		1818	68	1,692	31	1,593	25	93
11	280	458	0.61	0.0766	0.0043	1.6671	0.1052	0.1575	0.0035		1,109	111	996	40	943	19	106
12	125	234	0.54	0.1855	0.0061	11.4717	0.3940	0.4477	0.0074		2,703	56	2,562	32	2,385	33	95
13	87	158	0.55	0.0769	0.0047	1.4496	0.0931	0.1366	0.0036		1,118	134	910	39	825	20	110
14	224	352	0.64	0.0991	0.0040	3.3053	0.1592	0.2409	0.0046		1,606	75	1,482	38	1,391	24	107
15	60	87	0.70	0.1032	0.0053	3.8121	0.1936	0.2680	0.0058		1,683	94	1,595	41	1,531	30	95
16	211	333	0.64	0.0818	0.0032	2.0889	0.0946	0.1847	0.0052		1,243	77	1,145	31	1,093	28	105
17	209	164	1.28	0.0829	0.0047	2.2877	0.1370	0.1996	0.0047		1,266	110	1,209	42	1,173	25	103
18	132	135	0.97	0.1624	0.0088	10.1984	0.5231	0.4546	0.0084		2,481	93	2,453	48	2,416	37	99
19	182	213	0.86	0.1026	0.0043	3.8946	0.1596	0.2749	0.0058		1,672	78	1,613	33	1,566	29	96
20	247	365	0.68	0.1059	0.0051	3.5797	0.1709	0.2445	0.0044		1731	91	1,545	38	1,410	23	110
21	139	221	0.63	0.0815	0.0046	2.2472	0.1210	0.1996	0.0054		1,235	99	1,196	38	1,173	29	102
22	46	134	0.34	0.0744	0.0044	1.6634	0.1027	0.1618	0.0042		1,052	119	995	39	967	23	103
23	176	130	1.36	0.0913	0.0044	3.5480	0.1804	0.2818	0.0065		1,454	92	1,538	40	1,600	33	96
24	73	96	0.76	0.1041	0.0066	4.1139	0.2981	0.2852	0.0078		1,699	127	1,657	59	1,617	39	98
25	87	70	1.26	0.1002	0.0052	4.1232	0.2108	0.2988	0.0066		1,628	87	1,659	42	1,685	33	102
26	52	140	0.37	0.0830	0.0082	2.0577	0.2497	0.1770	0.0048		1,269	190	1,135	83	1,050	26	108
27	92	302	0.31	0.0961	0.0034	3.8430	0.1536	0.2897	0.0061		1,550	67	1,602	32	1,640	31	103
28	269	399	0.67	0.0566	0.0034	0.6322	0.0401	0.0809	0.0018		476	133	497	25	502	11	99
10	198	183	1.08	0.1055	0.0052	3.2701	0.1426	0.2254	0.0050		1724	91	1,474	34	1,311	26	112
Sandstone-20HNS34																	
1	224	346	0.65	0.1586	0.0017	9.12	0.12	0.4149	0.0056	0	2,439	18	2,349	12	2,237	26	96
2	56	76	0.74	0.1011	0.0035	3.76	0.14	0.2647	0.0052	0	1,624	66	1,578	31	1,513	26	97
3	62	248	0.25	0.1075	0.0019	4.385	0.087	0.2923	0.0032	0	1751	33	1711	15	1,653	16	98

(Continued on following page)

TABLE 1 | (*Continued*) Zircon U-Pb ages of gabbros and sediment blocks from the Huaniushan complex in the Beishan orogen, NW China.

Sample no.				Isotopic ratio							Isotopic age (Ma)						Con.
	Th	U	Th/U	$^{207}Pb/^{206}Pb$	2σ	$^{207}Pb/^{235}U$	2σ	$^{206}Pb/^{238}U$	2σ		$^{207}Pb/^{206}Pb$	2σ	$^{207}Pb/^{235}U$	2σ	$^{206}Pb/^{238}U$	2σ	%
4	70	170	0.41	0.0832	0.0024	2.287	0.073	0.1989	0.0032	0	1,268	61	1,204	22	1,169	17	103
5	152	340	0.45	0.1169	0.0014	5.302	0.069	0.3242	0.0043	0	1906	22	1868	11	1809	21	98
6	166	219	0.76	0.0955	0.0023	3.38	0.093	0.2545	0.0042	0	1,529	45	1,497	22	1,461	21	102
7	104	168	0.62	0.1075	0.0026	4.5	0.11	0.298	0.0046	0	1749	45	1729	20	1,681	23	99
8	91	183	0.50	0.0768	0.003	1.897	0.074	0.1761	0.0033	0	1,092	82	1,083	24	1,045	18	104
9	99	207	0.48	0.0994	0.002	3.78	0.1	0.2766	0.0041	0	1,614	40	1,586	22	1,574	21	98
10	56	160	0.35	0.0636	0.0026	1.009	0.04	0.1152	0.0018	0	684	87	705	20	703	10	100
11	85	110	0.77	0.1155	0.0029	5.02	0.13	0.3133	0.0054	0	1874	46	1819	22	1756	27	97
12	154	221	0.70	0.1092	0.002	4.454	0.098	0.2978	0.005	0	1780	34	1720	18	1,680	25	97
13	120	380	0.32	0.076	0.0015	1.872	0.039	0.1771	0.0026	0	1,097	37	1,070	14	1,051	14	102
14	52	147	0.35	0.0784	0.003	1.99	0.078	0.1854	0.0034	0	1,152	73	1,108	26	1,096	18	101
15	83	145	0.57	0.0652	0.0032	1.062	0.051	0.1176	0.0025	0	740	100	729	26	716	14	102
16	162	701	0.23	0.0758	0.0011	1.783	0.041	0.1708	0.0024	1	1,084	30	1,037	15	1,016	13	102
17	57	94	0.61	0.1157	0.0029	5.17	0.15	0.3252	0.0071	0	1880	46	1844	24	1814	34	98
18	306	594	0.52	0.0669	0.0014	1.288	0.03	0.1388	0.0016	1	822	44	839	13	837.8	9	100
19	109	253	0.43	0.0735	0.0032	1.493	0.077	0.1509	0.0032	1	1,004	88	923	32	906	18	102
20	20	40	0.51	0.0851	0.0059	2.36	0.15	0.2031	0.006	0	1,200	150	1,221	44	1,191	32	103
22	215	162	1.33	0.0851	0.0023	2.531	0.072	0.2161	0.0034	0	1,310	53	1,278	21	1,261	18	101
23	29	147	0.20	0.1258	0.0025	6.07	0.14	0.3462	0.0063	1	2033	36	1984	20	1915	30	98
24	220	228	0.96	0.1065	0.0018	4.16	0.11	0.2836	0.0036	1	1734	31	1,663	22	1,609	18	96
25	170	229	0.74	0.1038	0.0025	3.98	0.12	0.2823	0.0051	0	1,685	45	1,627	25	1,602	25	97
26	125	191	0.65	0.1112	0.0019	4.716	0.092	0.304	0.0043	0	1818	32	1768	16	1710	21	97
27	50	106	0.47	0.0774	0.0023	1.963	0.07	0.1834	0.0033	0	1,123	63	1,098	24	1,085	18	101
28	189	194	0.97	0.096	0.0022	3.561	0.098	0.27	0.0052	1	1,544	41	1,536	22	1,540	26	99
29	65	130	0.50	0.0702	0.0036	1.127	0.054	0.118	0.0023	0	880	110	761	26	719	13	106
30	27	67	0.40	0.0873	0.0045	2.7	0.13	0.2262	0.0047	0	1,322	97	1,319	35	1,314	25	100
31	75	164	0.46	0.091	0.0026	2.93	0.1	0.2374	0.0048	0	1,437	56	1,386	26	1,373	25	101
32	298	459	0.65	0.0796	0.0013	2.149	0.041	0.1954	0.0025	0	1,179	33	1,163	13	1,151	13	101
33	44	111	0.39	0.0668	0.0033	1.062	0.055	0.1164	0.0023	0	770	110	728	27	710	13	103
34	143	338	0.42	0.0836	0.0028	2.255	0.084	0.199	0.0048	0	1,272	66	1,196	27	1,170	26	102
35	67	166	0.40	0.0856	0.0033	2.501	0.09	0.2145	0.0051	0	1,320	70	1,268	26	1,252	27	101
36	150	347	0.43	0.1078	0.0017	4.431	0.077	0.2956	0.0036	0	1764	27	1717	14	1,669	18	97
37	186	362	0.51	0.1082	0.0017	4.701	0.084	0.3125	0.0039	1	1765	28	1766	15	1752	19	100
38	110	144	0.76	0.0844	0.0024	2.509	0.073	0.2148	0.0048	0	1,283	56	1,271	21	1,254	25	101
39	91	92	0.98	0.1175	0.0043	4.43	0.22	0.279	0.012	1	1904	67	1709	42	1,583	58	90
40	45	96	0.47	0.0832	0.0048	2.53	0.15	0.2166	0.0059	0	1,240	120	1,273	44	1,263	31	101
41	192	146	1.32	0.1016	0.0027	3.86	0.15	0.2791	0.0058	0	1,656	53	1,600	33	1,594	32	97
42	229	315	0.73	0.0643	0.002	1.051	0.032	0.1183	0.0019	0	726	66	727	16	721	11	101
43	203	347	0.59	0.0892	0.0021	2.933	0.092	0.2378	0.0049	1	1,399	46	1,388	23	1,375	25	101
44	409	659	0.62	0.0613	0.0012	0.867	0.019	0.1026	0.0014	0	638	44	633	10	629.3	8.2	101
45	156	142	1.10	0.1013	0.0036	3.72	0.14	0.2719	0.0057	0	1,631	64	1,572	29	1,550	29	96
46	80	191	0.42	0.0631	0.0021	1.048	0.042	0.1204	0.0021	0	681	73	724	21	733	12	99
47	104	131	0.80	0.113	0.0028	4.96	0.12	0.3175	0.0051	0	1835	47	1810	20	1777	25	99
48	177	169	1.05	0.0778	0.0025	1.954	0.065	0.1836	0.0032	0	1,129	59	1,095	22	1,086	17	101
49	368	444	0.83	0.0939	0.0014	3.38	0.11	0.2609	0.0053	1	1,500	28	1,495	25	1,493	27	100
50	101	251	0.40	0.1141	0.0019	5.19	0.1	0.3293	0.0041	0	1860	30	1849	17	1834	20	99
51	35	98	0.36	0.0975	0.0026	3.63	0.1	0.2718	0.0044	0	1,570	55	1,557	25	1,549	22	99
52	76	114	0.67	0.0896	0.0028	2.83	0.11	0.2306	0.0051	0	1,395	62	1,356	29	1,337	26	101
53	141	391	0.36	0.0516	0.002	0.351	0.017	0.04909	0.00085	0	259	89	307	13	308.9	5.2	99
54	68	90	0.75	0.1011	0.0039	3.83	0.15	0.2744	0.007	0	1,637	70	1,593	32	1,562	35	97
55	78	135	0.58	0.0644	0.0028	1.039	0.046	0.1167	0.0019	0	700	100	719	23	711	11	101
56	144	256	0.56	0.0806	0.0018	2.193	0.055	0.1985	0.003	0	1,199	45	1,176	18	1,167	16	101
57	114	129	0.88	0.1146	0.0025	5.23	0.12	0.3321	0.0058	0	1863	40	1854	19	1847	28	100
58	89	224	0.40	0.0901	0.0018	3.089	0.066	0.2484	0.0037	0	1,419	38	1,428	17	1,430	19	100
59	150	360	0.42	0.0756	0.0015	1.957	0.059	0.1861	0.003	1	1,081	41	1,097	20	1,100	16	100
60	527	352	1.50	0.0636	0.0019	1.048	0.031	0.12	0.0018	0	704	63	726	15	730	11	99
61	44	90	0.49	0.0771	0.0032	2.007	0.083	0.1898	0.0037	0	1,078	87	1,110	28	1,119	20	99
62	104	154	0.68	0.0877	0.0023	2.983	0.088	0.243	0.0041	0	1,361	50	1,399	22	1,402	21	100
63	31	83	0.37	0.0881	0.0027	2.822	0.099	0.2312	0.0042	0	1,363	58	1,355	26	1,340	22	101
64	6	146	0.04	0.1656	0.0024	11.03	0.23	0.4787	0.0079	1	2,510	24	2,522	20	2,520	35	100
65	134	213	0.63	0.0749	0.0018	1.832	0.047	0.1777	0.0029	0	1,052	49	1,058	16	1,054	16	100

(Continued on following page)

TABLE 1 | (*Continued*) Zircon U-Pb ages of gabbros and sediment blocks from the Huaniushan complex in the Beishan orogen, NW China.

Sample no.	Th	U	Th/U	Isotopic ratio							Isotopic age (Ma)						Con.
				$^{207}Pb/^{206}Pb$	2σ	$^{207}Pb/^{235}U$	2σ	$^{206}Pb/^{238}U$	2σ		$^{207}Pb/^{206}Pb$	2σ	$^{207}Pb/^{235}U$	2σ	$^{206}Pb/^{238}U$	2σ	%
66	160	146	1.10	0.0792	0.003	2.183	0.079	0.1993	0.0035	0	1,156	73	1,175	24	1,174	18	100
67	203	251	0.81	0.0971	0.0018	3.662	0.091	0.2729	0.004	1	1,569	34	1,560	20	1,555	20	100
68	53	84	0.63	0.085	0.003	2.619	0.095	0.2242	0.0044	0	1,284	72	1,299	27	1,303	23	100
69	94	79	1.19	0.0982	0.0032	3.69	0.13	0.2729	0.0058	0	1,565	63	1,567	28	1,554	29	100
70	92	138	0.67	0.0934	0.0038	2.96	0.12	0.2406	0.0064	0	1,480	75	1,394	29	1,389	33	100
71	136	444	0.31	0.0582	0.0018	0.651	0.022	0.0811	0.0013	0	510	69	510	13	502.5	7.8	101
72	46	83	0.55	0.1045	0.0028	4.38	0.13	0.2986	0.0058	0	1709	49	1703	24	1,683	29	100
73	179	275	0.65	0.1027	0.0018	4.23	0.1	0.2948	0.0038	1	1,671	34	1,676	20	1,665	19	100
74	42	33	1.28	0.1173	0.0047	5.65	0.24	0.3461	0.0081	0	1883	74	1918	39	1914	39	102
75	43	59	0.72	0.0788	0.0037	2.08	0.1	0.1914	0.0039	0	1,132	99	1,134	34	1,128	21	101
76	76	112	0.68	0.0755	0.0036	1.96	0.1	0.1849	0.0052	0	1,050	100	1,094	36	1,093	28	100
77	188	310	0.61	0.0798	0.0024	2.36	0.068	0.2097	0.0039	0	1,179	61	1,229	21	1,227	21	100
78	205	268	0.76	0.0703	0.0019	1.486	0.043	0.1533	0.0023	0	919	55	922	17	922	14	100
79	117	121	0.97	0.0972	0.0023	3.72	0.11	0.2747	0.0042	0	1,559	45	1,571	23	1,564	21	101
80	84	177	0.47	0.1093	0.0025	4.88	0.11	0.3177	0.0048	0	1786	38	1800	18	1782	22	101
81	38	64	0.60	0.1171	0.004	5.53	0.2	0.3428	0.0076	0	1891	62	1897	31	1899	36	100
82	99	211	0.47	0.115	0.0019	5.39	0.11	0.3396	0.0049	0	1884	27	1881	17	1884	24	100
83	235	292	0.80	0.1043	0.0017	4.59	0.093	0.3139	0.0043	1	1706	29	1745	17	1759	21	102
84	50	121	0.41	0.0777	0.0026	2.015	0.073	0.1861	0.0041	0	1,126	66	1,115	25	1,100	22	101
85	39	99	0.39	0.0906	0.0034	3.21	0.11	0.2545	0.0051	0	1,407	73	1,453	27	1,461	26	99
86	229	254	0.90	0.1626	0.0029	10.41	0.23	0.4595	0.0097	1	2,479	30	2,470	20	2,436	43	100
87	178	144	1.24	0.0707	0.0028	1.55	0.066	0.1585	0.0034	0	908	81	944	26	948	19	100
88	106	447	0.24	0.0712	0.0015	1.544	0.042	0.1567	0.0021	1	959	42	948	16	938	12	101
89	535	285	1.88	0.0923	0.0031	3.04	0.14	0.2445	0.0054	1	1,483	54	1,414	36	1,410	28	100
90	63	187	0.34	0.1809	0.0032	12.23	0.37	0.498	0.01	1	2,657	29	2,617	30	2,605	44	98
21	1,150	845	1.36	0.12	0.0039	3.42	0.15	0.203	0.007	1	1966	48	1,506	33	1,191	38	77

Carboniferous to Triassic (Zuo et al., 1990; Zuo et al., 1991; Nie et al., 2002a; Zhang et al., 2010; Zhang et al., 2011; Song et al., 2016; Tian and Xiao, 2020; Zheng et al., 2020).

The Liuyuan accretionary complex, located south of the Huaniushan arc (**Figure 1C**), contains the Liuyuan, Houhongquan, Huaniushan, Zhangfanshan, Huitongshan complex, and Gubaoquan eclogite. These ophiolitic complexes contain metamorphic basalts, gabbros, hornblendites, ultramafic rocks, cherts, limestones, sediments, and metamorphic tectonic blocks (Zuo et al., 1991; Liu & Wang, 1995; Xiao et al., 2010; Mao et al., 2012b; Wang et al., 2016). The Huaniushan complex is located in the northernmost part of the Liuyuan accretionary complex along the Huaniushan fault (**Figure 1C** and **Figure 2**).

FIELD CHARACTERS AND SAMPLING

Field Characters

In order to understand the composition and structure of the Huaniushan complex, we mapped in detail based on the previous map data (GSBGMR, 1989). The main lithologies and structures that are representative of the complex are described below.

The Huaniushan complex has a block-in-matrix structure in which blocks of ultramafic rocks, gabbros, massive basalt, diabase dykes, cherts, limestone, and sandstone/siltstone embedded and imbricated in a matrix of chlorite–phyllite schist and cleaved sandstone (**Figures 2–4**), which should be renamed as the Huaniushan ophiolitic mélange.

The Huaniushan ophiolitic mélange contains oceanic fragments which were thrusted on the calcareous sediments and volcanic and volcaniclastic rocks or emplaced into sedimentary matrix as large blocks (**Figures 2–5**). The Huaniushan complex mainly comprises basalt blocks and a few blocks of ultramafic rocks, gabbros, basalt, thinly bedded cherts, limestones, and tuff sandstones (**Figure 4**). Ultramafic blocks are located along the fault on the southwestern margin of the complex (**Figures 2**, **3**), and are cleaved (**Figure 4A**). A few gabbros develop along the southern and northern boundary fault in the eastern parts of the complex (**Figures 2**, **3**, **4B**). We found a NW-trending chert + limestone+ tuff sandstone layer in the middle of the complex (**Figures 3**, **4D–F**), namely, the thin chert cover on the basalts, the laminated limestone cover the cherts, and finally, the tuff sandstone lay on the limestone as shown in **Figures 4D, F**. The matrix limestone, sandstones, and chlorite–phyllites are highly cleaved (**Figures 4**, **5**). The southern part Huaniushan Formation (O_2*hn*) matrix calcareous sediments and volcanic and volcaniclastic rocks develop folds and EW-trending subvertical cleavage (**Figure 5C**). The central parts of the complex (containing the basalt, ultramafic gabbro, and sediments) also underwent subvertical cleavage (**Figures 4A, C, F**), and the gabbro also comprised gneisses (**Figure 5D**). The EW-trending, subvertical cleavage in the matrix in the northern parts of the complex is penetrative and has overprinted the bedding so strongly that the primary depositional structures are mostly difficult to observe (**Figures**

TABLE 2 | Data of zircon Lu-Hf isotopes for the Huaniushan complex in the Beishan orogen.

Sample no.	t (Ma)	$^{176}Yb/^{177}Hf$	$^{176}Lu/^{177}Hf$	$^{176}Hf/^{177}Hf$	2σ	$^{176}Hf/^{177}Hfi$	$^{176}Hf/^{177}Hfi(DM)$	$\varepsilon_{Hf}(t)$	$T_{DM1}(Hf)$	$T_{DM2}(Hf)$	$f_{Lu/Hf}$
					Gabbro (20HNS27)						
1	508.1	0.459011	0.014536	0.283097	0.000026	*0.282957*	0.282884	17.7	346	343	−0.56
2	502.5	0.238051	0.007914	0.282831	0.000034	*0.282754*	0.282888	10.4	736	807	−0.76
3	492.8	0.297386	0.009144	0.282957	0.000026	*0.282871*	0.282895	14.3	538	549	−0.72
4	496.9	0.243924	0.007577	0.282951	0.000026	*0.282879*	0.282892	14.7	521	528	−0.77
5	495.4	0.333747	0.010600	0.282932	0.000026	*0.282832*	0.282894	13.0	613	635	−0.68
6	508.1	0.231286	0.007327	0.282829	0.000025	*0.282757*	0.282884	10.7	725	796	−0.78
7	504	0.263958	0.008101	0.282913	0.000024	*0.282835*	0.282887	13.3	596	623	−0.76
8	499.9	0.366898	0.011795	0.282865	0.000028	*0.282752*	0.282890	10.3	775	813	−0.64
9	508.8	0.148895	0.004555	0.282826	0.000022	*0.282781*	0.282884	11.5	671	743	−0.86
10	504.5	0.246870	0.008110	0.282967	0.000030	*0.282889*	0.282887	15.2	502	501	−0.76
11	502	0.366841	0.011684	0.282947	0.000031	0.282836	0.282889	13.3	608	623	−0.65
12	500.5	0.439932	0.013828	0.283021	0.000028	0.282889	0.282890	15.2	502	502	−0.58
13	493.9	0.196293	0.006274	0.282885	0.000027	0.282825	0.282895	12.7	610	653	−0.81
14	507	0.026481	0.000998	0.282887	0.000012	0.282875	0.282885	14.8	521	530	−0.97
15	513	0.305290	0.009138	0.282928	0.000025	0.282838	0.282881	13.6	591	611	−0.72
16	505	0.121992	0.004239	0.282861	0.000028	0.282819	0.282887	12.8	611	659	−0.87
17	510.3	0.372396	0.011260	0.282903	0.000029	0.282794	0.282883	12.0	684	712	−0.66
18	510.3	0.463532	0.014853	0.283086	0.000032	0.282942	0.282883	17.3	377	376	−0.55
19	513.4	0.023527	0.000868	0.282691	0.000016	0.282680	0.282881	8.1	796	966	−0.97
20	517.6	0.180370	0.006038	0.282838	0.000025	0.282777	0.282878	11.6	682	744	−0.82
					Sandstone (20HNS34)						
1	2,439	0.045337	0.001516	0.281362	0.000016	0.281289	0.281463	2.2	2,680	2,819	−0.95
2	1,624	0.038767	0.001349	0.282017	0.000013	0.281973	0.282069	7.9	1758	1837	−0.96
3	1751	0.049379	0.001745	0.282019	0.000023	0.281959	0.281975	10.3	1774	1788	−0.95
4	1,169	0.043961	0.001569	0.282289	0.000016	0.282252	0.282404	7.5	1,385	1,508	−0.95
5	1906	0.041998	0.001523	0.281974	0.000014	0.281917	0.281860	12.3	1826	1780	−0.95
6	1,461	0.022578	0.000835	0.281663	0.000015	0.281638	0.282189	−7.7	2,221	2,681	−0.97
7	1749	0.017325	0.000645	0.282354	0.000015	0.282331	0.281977	23.4	1,260	960	−0.98
8	1,045	0.028360	0.001020	0.281646	0.000018	0.281624	0.282494	−17.5	2,255	2,978	−0.97
9	1,614	0.042864	0.001563	0.281783	0.000014	0.281733	0.282077	−0.9	2096	2,374	−0.95
10	703	0.024612	0.000822	0.282446	0.000017	0.282433	0.282743	3.5	1,138	1,401	−0.98
11	1874	0.026718	0.000982	0.281471	0.000014	0.281434	0.281884	−5.6	2,494	2,865	−0.97
12	1780	0.017934	0.000640	0.281486	0.000019	0.281462	0.281954	−6.7	2,451	2,863	−0.98
13	1,051	0.016263	0.000596	0.282307	0.000016	0.282294	0.282490	6.3	1,323	1,491	−0.98
14	1,096	0.013061	0.000477	0.282145	0.000016	0.282134	0.282457	1.7	1,542	1819	−0.99
15	716	0.034993	0.001175	0.282485	0.000019	0.282467	0.282734	5.0	1,094	1,318	−0.96
16	1,016	0.033672	0.001069	0.282302	0.000015	0.282280	0.282515	5.1	1,347	1,545	−0.97
17	1880	0.031317	0.001077	0.281549	0.000017	0.281508	0.281880	−2.8	2,393	2,698	−0.97
18	837.8	0.041853	0.001463	0.282203	0.000019	0.282178	0.282645	−2.5	1,502	1886	−0.96
19	906	0.042877	0.001521	0.282175	0.000019	0.282147	0.282596	−2.1	1,544	1911	−0.95
20	1,191	0.024673	0.000915	0.282066	0.000019	0.282044	0.282388	0.6	1,670	1958	−0.97
21	1966	0.106833	0.003387	0.281595	0.000015	0.281466	0.281816	−2.3	2,480	2,735	−0.90
22	1,261	0.047560	0.001729	0.282165	0.000015	0.282122	0.282336	5.0	1,567	1740	−0.95
23	2033	0.016822	0.000588	0.281675	0.000026	0.281651	0.281766	5.7	2,190	2,287	−0.98
24	1734	0.010713	0.000513	0.281461	0.000018	0.281442	0.281988	−8.5	2,477	2,937	−0.98
25	1,685	0.014051	0.000498	0.281398	0.000019	0.281380	0.282024	−11.8	2,561	3,104	−0.99
26	1818	0.049880	0.001913	0.281822	0.000019	0.281754	0.281926	4.5	2062	2,198	−0.94
27	1,085	0.044816	0.001534	0.282262	0.000029	0.282228	0.282465	4.8	1,421	1,615	−0.95
28	1,544	0.022018	0.000809	0.281910	0.000018	0.281884	0.282128	2.9	1881	2086	−0.98
29	719	0.044367	0.001523	0.282424	0.000020	0.282402	0.282732	2.8	1,190	1,462	−0.95
30	1,314	0.029463	0.001069	0.282138	0.000017	0.282109	0.282297	5.7	1,577	1734	−0.97
31	1,373	0.047238	0.001652	0.282204	0.000023	0.282159	0.282254	8.8	1,508	1,585	−0.95
32	1,151	0.056300	0.001910	0.282275	0.000018	0.282231	0.282417	6.4	1,417	1,566	−0.94
33	710	0.026292	0.000906	0.282385	0.000019	0.282371	0.282738	1.5	1,226	1,537	−0.97
34	1,170	0.064155	0.002329	0.282265	0.000014	0.282212	0.282403	6.1	1,447	1,598	−0.93
35	1,252	0.054687	0.002005	0.282171	0.000016	0.282121	0.282343	4.7	1,570	1746	−0.94
36	1764	0.026805	0.000969	0.281595	0.000015	0.281560	0.281966	−3.6	2,323	2,658	−0.97
37	1765	0.035074	0.001303	0.281585	0.000021	0.281539	0.281965	−4.3	2,357	2,704	−0.96
38	1,254	0.029616	0.001084	0.282079	0.000021	0.282051	0.282341	2.3	1,660	1901	−0.97
39	1904	0.012785	0.000414	0.281532	0.000021	0.281515	0.281862	−2.0	2,375	2,668	−0.99

(Continued on following page)

TABLE 2 | (*Continued*) Data of zircon Lu-Hf isotopes for the Huaniushan complex in the Beishan orogen.

Sample no.	t (Ma)	$^{176}Yb/^{177}Hf$	$^{176}Lu/^{177}Hf$	$^{176}Hf/^{177}Hf$	2σ	$^{176}Hf/^{177}Hfi$	$^{176}Hf/^{177}Hfi(DM)$	$\varepsilon_{Hf}(t)$	$T_{DM1}(Hf)$	$T_{DM2}(Hf)$	$f_{Lu/Hf}$
40	1,263	0.034100	0.001386	0.282214	0.000017	0.282179	0.282335	7.0	1,483	1,611	−0.96
41	1,656	0.035815	0.001370	0.281838	0.000015	0.281793	0.282046	2.2	2010	2,216	−0.96
42	721	0.066287	0.002129	0.282439	0.000019	0.282408	0.282730	3.0	1,189	1,446	−0.94
43	1,375	0.071570	0.002496	0.282156	0.000019	0.282089	0.282253	6.4	1,612	1739	−0.92
44	629.3	0.028656	0.001040	0.282453	0.000017	0.282438	0.282797	2.1	1,135	1,437	−0.97
45	1,631	0.045135	0.001648	0.281970	0.000018	0.281917	0.282064	6.1	1838	1957	−0.95
46	733	0.019499	0.000696	0.282373	0.000015	0.282361	0.282721	1.6	1,236	1,543	−0.98
47	1835	0.017122	0.000607	0.281389	0.000015	0.281365	0.281913	−8.9	2,581	3,039	−0.98
48	1,086	0.028682	0.001080	0.281953	0.000017	0.281928	0.282464	−5.8	1835	2,281	−0.97
49	1,500	0.036190	0.001334	0.281993	0.000015	0.281953	0.282161	4.4	1791	1961	−0.96
50	1860	0.014957	0.000526	0.281557	0.000014	0.281536	0.281895	−2.3	2,348	2,650	−0.98
51	1,570	0.025606	0.000950	0.281867	0.000015	0.281837	0.282109	1.8	1947	2,173	−0.97
52	1,337	0.054598	0.002029	0.282195	0.000019	0.282142	0.282280	7.4	1,535	1,645	−0.94
53	308.9	0.030351	0.001289	0.282457	0.000015	0.282448	0.283028	−4.7	1,136	1,620	−0.96
54	1,637	0.065283	0.002444	0.282035	0.000016	0.281957	0.282060	7.6	1785	1865	−0.93
55	711	0.031658	0.001009	0.282459	0.000016	0.282444	0.282737	4.1	1,125	1,372	−0.97
56	1,167	0.068692	0.002486	0.282332	0.000020	0.282275	0.282405	8.3	1,356	1,457	−0.93
57	1863	0.057193	0.002184	0.281749	0.000015	0.281670	0.281892	2.6	2,180	2,353	−0.93
58	1,430	0.019049	0.000716	0.282065	0.000016	0.282043	0.282212	6.0	1,663	1806	−0.98
59	1,100	0.014775	0.000506	0.282248	0.000015	0.282235	0.282454	5.4	1,403	1,590	−0.98
60	730	0.098049	0.002878	0.282206	0.000022	0.282165	0.282724	−5.4	1,556	1984	−0.91
61	1,119	0.021732	0.000759	0.282252	0.000015	0.282234	0.282440	5.8	1,406	1,580	−0.98
62	1,402	0.040078	0.001379	0.282037	0.000015	0.281999	0.282233	3.8	1731	1922	−0.96
63	1,340	0.019119	0.000719	0.282212	0.000019	0.282192	0.282278	9.2	1,459	1,532	−0.98
64	2,510	0.029577	0.000917	0.281337	0.000044	0.281291	0.281410	3.9	2,671	2,768	−0.97
65	1,054	0.044538	0.001449	0.282311	0.000020	0.282280	0.282488	5.9	1,349	1,520	−0.96
66	1,174	0.022609	0.000837	0.282110	0.000019	0.282089	0.282400	1.9	1,606	1868	−0.97
67	1,555	0.075012	0.002627	0.282060	0.000017	0.281981	0.282120	6.6	1758	1865	−0.92
68	1,303	0.073030	0.002664	0.282254	0.000020	0.282186	0.282305	8.2	1,477	1,569	−0.92
69	1,565	0.026538	0.001042	0.281932	0.000016	0.281899	0.282113	3.9	1862	2039	−0.97
70	1,389	0.024139	0.000925	0.282093	0.000021	0.282066	0.282242	5.9	1,634	1781	−0.97
71	502.5	0.128655	0.005056	0.282802	0.000020	0.282753	0.282888	10.4	718	810	−0.85
72	1709	0.032067	0.001129	0.281758	0.000019	0.281720	0.282006	0.8	2,107	2,343	−0.97
73	1,671	0.059336	0.002365	0.281898	0.000017	0.281821	0.282034	3.6	1978	2,143	−0.93
74	1883	0.013638	0.000512	0.281306	0.000014	0.281286	0.281878	−10.6	2,685	3,182	−0.98
75	1,128	0.013323	0.000489	0.281938	0.000016	0.281926	0.282434	−5.0	1826	2,260	−0.99
76	1,093	0.024525	0.000890	0.282259	0.000013	0.282239	0.282459	5.3	1,401	1,587	−0.97
77	1,227	0.040381	0.001389	0.282287	0.000017	0.282252	0.282361	8.8	1,381	1,470	−0.96
78	922	0.038808	0.001344	0.282241	0.000014	0.282216	0.282584	0.7	1,443	1748	−0.96
79	1,559	0.019909	0.000741	0.281968	0.000015	0.281944	0.282117	5.4	1798	1943	−0.98
80	1786	0.028129	0.001010	0.281602	0.000016	0.281565	0.281949	−2.9	2,316	2,633	−0.97
81	1891	0.014390	0.000521	0.281555	0.000017	0.281535	0.281872	−1.6	2,349	2,633	−0.98
82	1884	0.028855	0.000954	0.281565	0.000021	0.281529	0.281877	−2.0	2,362	2,649	−0.97
83	1706	0.028012	0.001028	0.281748	0.000018	0.281713	0.282009	0.5	2,115	2,359	−0.97
84	1,100	0.032370	0.001119	0.282325	0.000016	0.282300	0.282454	7.7	1,317	1,446	−0.97
85	1,461	0.023835	0.000852	0.281991	0.000017	0.281966	0.282189	3.9	1771	1958	−0.97
86	2,479	0.035947	0.001119	0.281345	0.000023	0.281290	0.281433	3.2	2,675	2,792	−0.97
87	948	0.055335	0.001964	0.282218	0.000014	0.282181	0.282565	0.1	1,500	1807	−0.94
88	938	0.063793	0.002221	0.282269	0.000016	0.282228	0.282572	1.5	1,437	1709	−0.93
89	1,410	0.047699	0.001623	0.282030	0.000021	0.281984	0.282227	3.4	1753	1950	−0.95
90	2,657	0.017240	0.000739	0.281141	0.000015	0.281102	0.281299	0.6	2,924	3,087	−0.98

5G, H). And, they were intruded by the Huaniushan granite in the late Triassic and formed the skarn-type Pb-Zn mineralization (**Figure 2**).

Sampling

Thirty samples (twenty-two basalt and eight gabbros) were collected from the outcrops (**Figures 2**, **3**) for major and trace element analyses.

Peridotite is dark gray and strong serpentinized and develops EW-trending foliations with network structures. It mainly consists of serpentine, a few pyroxenes, and magnetite (**Figure 4A**). Gabbro samples are gray and have altered display (**Figures 4B,G**). The gabbros in the faults are strongly deformed (**Figure 5D**). They are characterized by fine-to medium-grained hypidiomorphic textures and mainly contain plagioclase (55–65 vol%), clinopyroxene (30–35 vol%), and olivine (2-3 vol%), with minor amphibole and Fe-Ti oxides (**Figure 4G**). Most basalt are gray, massive, and altered, and the schist basalts are located along the faults (**Figures 4C,D**).

TABLE 3 | Major (wt%) and trace element (ppm) results for the Huaniushan complex in the Beishan orogen, NW China.

Sample no.	11HN03-1	11HN03-5	11HN08-1	11HN08-4	11HN09-1	11HN09-4	06LY09-1	06LY09-2	06LY10-1	06LY10-2	06LY11-1	06LY11-2	06LY11-3	18HNS02-1	18HNS05-2
Rock type	Basalt														
SiO_2	49.64	48.89	49.51	44.08	50.22	51.22	45.98	48.80	49.48	47.09	48.41	46.90	47.99	50.42	47.73
TiO_2	0.97	1.45	1.34	0.65	1.27	1.14	0.55	0.83	1.28	1.11	1.16	1.01	1.16	1.11	1.37
Al_2O_3	13.78	13.29	13.93	11.43	13.12	12.73	11.75	14.21	12.59	13.58	13.43	12.84	13.02	13.84	13.05
Fe_2O_{3T}	11.88	14.53	14.04	10.79	13.63	13.30	10.45	10.87	14.16	12.29	12.40	11.61	13.08		13.88
MnO	0.18	0.22	0.23	0.18	0.20	0.23	0.18	0.20	0.23	0.22	0.22	0.20	0.19	0.17	0.18
MgO	8.28	6.25	6.87	18.17	7.56	6.46	16.24	8.24	7.12	8.23	7.61	10.24	8.61	7.96	9.90
CaO	10.58	12.01	10.31	9.50	10.48	11.48	10.14	13.63	11.00	13.98	11.98	11.14	12.07	10.04	8.83
Na_2O	2.96	2.39	2.60	0.75	2.47	2.36	1.01	2.17	2.94	1.86	2.74	2.57	1.87	2.76	2.86
K_2O	0.08	0.10	0.21	0.21	0.13	0.13	0.38	0.13	0.15	0.26	0.45	0.20	0.18	0.40	0.44
P_2O_5	0.07	0.11	0.11	0.05	0.09	0.09	0.04	0.07	0.08	0.08	0.10	0.07	0.09	0.09	0.11
LOI	1.51	0.72	0.83	4.01	0.79	0.80	2.80	0.48	0.59	0.88	1.08	2.76	1.31	0.82	1.56
Total	99.93	99.96	99.97	99.81	99.96	99.93	99.52	99.63	99.62	99.58	99.58	99.54	99.57	87.61	99.90
Sc	46.20	46.40	50.10	35.40	50.30	45.30	27.87	34.91	56.80	53.70	54.40	52.40	52.30	31.94	28.32
V	280	365	365	217	354	331			387	344	352	306	354	342	373
Cr	313	104	165	1,303	171	158		272	239	0	311	453	359	225	459
Co	49	52	52	74	52	49	58	36	52	44	46	46	46	49	55
Ni	126	71	83	649	91	83	474	86	125	136	109	190	154	113	235
Ga	10.80	18.20	16.40	11.10	15.10	15.10	9.62	12.50	17.00	16.20	15.30	12.20	13.80	16.71	17.00
Rb	0.88	0.55	3.13	1.22	3.58	2.11	19.05	0.53	2.71	7.00	25.60	9.20	5.73	14.53	9.61
Sr	111	99	116	37	121	143	130	176	90	152	207	143	117	369	160
Y	20.80	29.40	29.70	15.70	26.90	25.70	12.29	16.30	26.40	22.30	24.30	20.50	23.30	22.25	27.78
Nb	2.06	4.20	4.04	1.35	3.09	2.78	1.53	2.26	3.50	2.50	2.94	2.27	2.64	4.32	4.90
Cs	0.39	0.06	0.38	0.13	0.46	0.41	6.16	0.16	0.30	0.72	2.87	1.71	0.74	3.75	3.69
Ba	42	38	108	48	56	42	67	21	47	50	74	64	70	595	417
La	2.94	5.19	5.36	1.85	4.25	3.78	1.16	2.22	4.88	3.84	4.41	3.32	4.15	5.09	5.90
Ce	7.34	13.20	13.30	5.37	10.90	9.98	3.31	5.94	11.70	8.99	10.20	8.22	9.27	14.64	15.61
Pr	1.14	2.00	1.98	0.85	1.61	1.48	0.52	0.89	1.75	1.49	1.70	1.32	1.63	1.83	2.27
Nd	6.13	10.20	10.00	4.83	8.54	7.87	2.87	4.82	8.65	7.70	8.75	6.84	8.02	8.92	11.02
Sm	1.74	3.20	3.35	1.23	2.54	2.72	1.06	1.62	2.74	2.37	2.81	2.27	2.63	2.66	3.32
Eu	0.73	1.13	1.09	0.61	0.90	1.00	0.43	0.65	0.98	0.97	1.05	0.79	0.88	1.19	1.35
Gd	2.60	3.55	4.04	2.08	3.55	3.42	1.47	2.04	3.75	3.36	3.54	2.92	3.32	2.88	3.62
Tb	0.57	0.86	0.81	0.37	0.73	0.70	0.28	0.38	0.69	0.61	0.62	0.53	0.62	0.58	0.74
Dy	3.46	4.86	5.28	2.85	5.00	4.44	2.11	2.84	4.49	3.92	4.22	3.56	4.18	3.85	4.82
Ho	0.77	1.03	1.08	0.54	0.98	0.95	0.40	0.60	1.00	0.84	0.92	0.81	0.89	0.79	0.99
Er	2.44	3.31	3.38	1.93	3.30	3.11	1.24	1.56	3.04	2.65	2.66	2.33	2.55	3.02	3.46
Tm	0.41	0.51	0.55	0.28	0.53	0.47	0.20	0.26	0.43	0.36	0.39	0.33	0.35	0.38	0.48
Yb	2.36	3.24	3.41	1.83	2.97	2.85	1.23	1.70	2.71	2.29	2.56	2.23	2.40	2.39	3.00
Lu	0.38	0.48	0.49	0.26	0.44	0.36	0.19	0.27	0.45	0.37	0.36	0.32	0.35	0.34	0.43
Zr	72.90	94.20	55.10	57.90	56.90	57.60	21.77	33.59	74.50	82.20	67.50	56.50	53.90	124.50	139.70
Hf	1.97	3.18	2.01	1.47	2.05	2.06	0.73	1.20	2.75	2.91	2.57	2.13	2.25	3.21	3.81
Ta	0.16	0.26	0.23	0.10	0.17	0.19	0.15	0.17	0.20	0.15	0.19	0.15	0.17	0.73	0.75
Pb	12.20	7.15	10.40	9.39	11.70	5.81	8.35	18.43	15.30	11.50	17.20	14.70	12.70	10.65	17.20
Th	0.27	0.47	0.51	0.18	0.42	0.35	0.10	0.23	0.63	0.39	0.50	0.41	0.44	0.58	0.63
U	0.10	0.23	0.23	0.09	0.18	0.19	0.02	0.07	0.17	0.18	0.16	0.14	0.17	0.23	0.20

Sample no.	18HNS09-1	18HNS09-2	18HNS04-2	18HNS04-3	18HNS04-5	18HNS10-2	18HNS10-3	18HNS12-2	18HNS13	06LY12-1	06LY12-2
Rock type	Basalt		Gabbro							Basalt	
SiO_2	50.25	48.52	47.57	46.57	47.96	49.19	46.81	48.63	46.58	46.97	46.99

(Continued on following page)

TABLE 3 | (*Continued*) Major (wt%) and trace element (ppm) results for the Huaniushan complex in the Beishan orogen, NW China.

Sample no.	18HNS09-1	18HNS09-2	18HNS04-2	18HNS04-3	18HNS04-5	18HNS10-2	18HNS10-3	18HNS12-2	18HNS13	06LY12-1	06LY12-2
Rock type	Basalt		Gabbro							Basalt	
TiO_2	0.82	1.04	1.47	1.32	1.40	1.31	0.64	1.13	0.55	2.48	2.57
Al_2O_3	14.32	15.01	16.09	17.04	16.61	17.83	15.97	15.62	10.46	8.59	9.06
Fe_2O_{3T}	11.46	13.31	10.51	11.28	11.13	9.07	10.77	12.96	10.96	16.27	13.98
MnO	0.17	0.18	0.19	0.17	0.15	0.17	0.20	0.21	0.15	0.20	0.24
MgO	8.51	7.47	9.06	8.43	9.12	6.84	9.74	7.95	16.95	10.91	12.67
CaO	9.92	10.61	11.00	12.14	8.40	10.72	10.87	9.38	9.20	10.51	10.74
Na_2O	3.39	2.67	2.01	1.47	3.29	3.11	2.88	2.66	1.48	2.01	1.55
K_2O	0.13	0.07	0.34	0.32	0.27	0.47	0.63	0.32	0.06	0.19	0.25
P_2O_5	0.08	0.09	0.13	0.12	0.12	0.12	0.07	0.09	0.06	0.18	0.19
LOI	0.87	0.94	1.54	1.05	1.44	1.08	1.32	0.98	3.39	1.26	1.34
Total	99.92	99.91	99.91	99.93	99.90	99.90	99.90	99.92	99.85	99.57	99.58
Sc	29.82	32.10	28.34	29.47	28.95	26.71	26.32	29.50	29.93	29.00	29.20
V	307	364	244	227	210	206	158	307	212	220	253
Cr	311	230	318	313	309	369	389	143	1,535	828	656
Co	47	48	40	45	40	37	44	52	68	70	53
Ni	124	105	113	103	113	72	158	119	623	532	447
Ga	14.20	22.24	14.43	21.89	15.97	18.39	14.72	16.55	10.68	14.00	17.10
Rb	5.38	9.38	17.25	18.02	28.33	17.95	23.44	9.56	13.19	3.06	5.53
Sr	101	303	152	59	100	174	282	107	79	262	183
Y	20.30	23.97	24.29	23.89	22.30	21.39	16.19	22.27	13.27	22.10	23.20
Nb	2.62	3.68	5.32	5.08	4.70	4.57	2.19	4.48	1.80	14.50	14.70
Cs	1.86	3.44	5.12	4.33	5.67	4.35	4.59	3.75	3.91	0.45	1.53
Ba	467	487	519	515	527	510	575	81	536	80	74
La	3.63	4.60	6.66	6.65	6.52	6.71	3.35	5.29	2.38	15.40	15.90
Ce	10.55	14.27	18.82	18.67	19.26	18.35	9.58	11.59	9.63	33.20	34.80
Pr	1.36	1.68	2.49	2.41	2.40	2.38	1.22	1.86	0.87	4.82	4.98
Nd	6.73	8.21	12.03	11.64	11.32	11.34	6.16	8.93	4.44	22.30	23.20
Sm	2.16	2.61	3.47	3.38	3.20	3.21	1.94	2.69	1.44	5.26	5.64
Eu	0.91	1.24	1.41	1.55	1.40	1.37	0.75	0.81	0.74	1.71	1.89
Gd	2.35	2.85	3.72	3.49	3.35	3.27	1.99	2.76	1.66	5.72	5.78
Tb	0.50	0.60	0.72	0.67	0.63	0.63	0.41	0.58	0.34	0.83	0.88
Dy	3.39	4.01	4.63	4.31	3.99	3.99	2.75	3.86	2.32	4.58	4.83
Ho	0.70	0.84	0.91	0.86	0.79	0.79	0.56	0.79	0.48	0.81	0.84
Er	2.70	2.89	2.90	2.75	2.68	2.59	1.86	2.36	1.84	2.12	2.16
Tm	0.35	0.41	0.42	0.39	0.36	0.36	0.27	0.39	0.24	0.28	0.27
Yb	2.21	2.67	2.60	2.43	2.27	2.22	1.70	2.46	1.49	1.54	1.60
Lu	0.32	0.39	0.37	0.35	0.31	0.31	0.24	0.36	0.22	0.20	0.21
Zr	135.20	117.30	127.50	145.70	128.00	150.20	75.29	148.10	52.35	94.60	105.00
Hf	3.62	3.31	3.59	3.90	3.51	3.88	2.11	3.89	1.60	3.49	3.26
Ta	0.44	0.65	1.05	1.67	1.81	0.61	0.54	0.49	0.70	0.88	0.91
Pb	19.75	9.92	18.32	14.97	15.20	29.40	38.58	15.50	12.58	33.00	50.20
Th	0.41	0.50	0.61	0.57	0.58	0.53	0.38	0.56	0.32	1.26	1.22
U	0.18	0.31	0.25	0.26	0.25	0.24	0.29	0.21	0.21	0.29	0.32

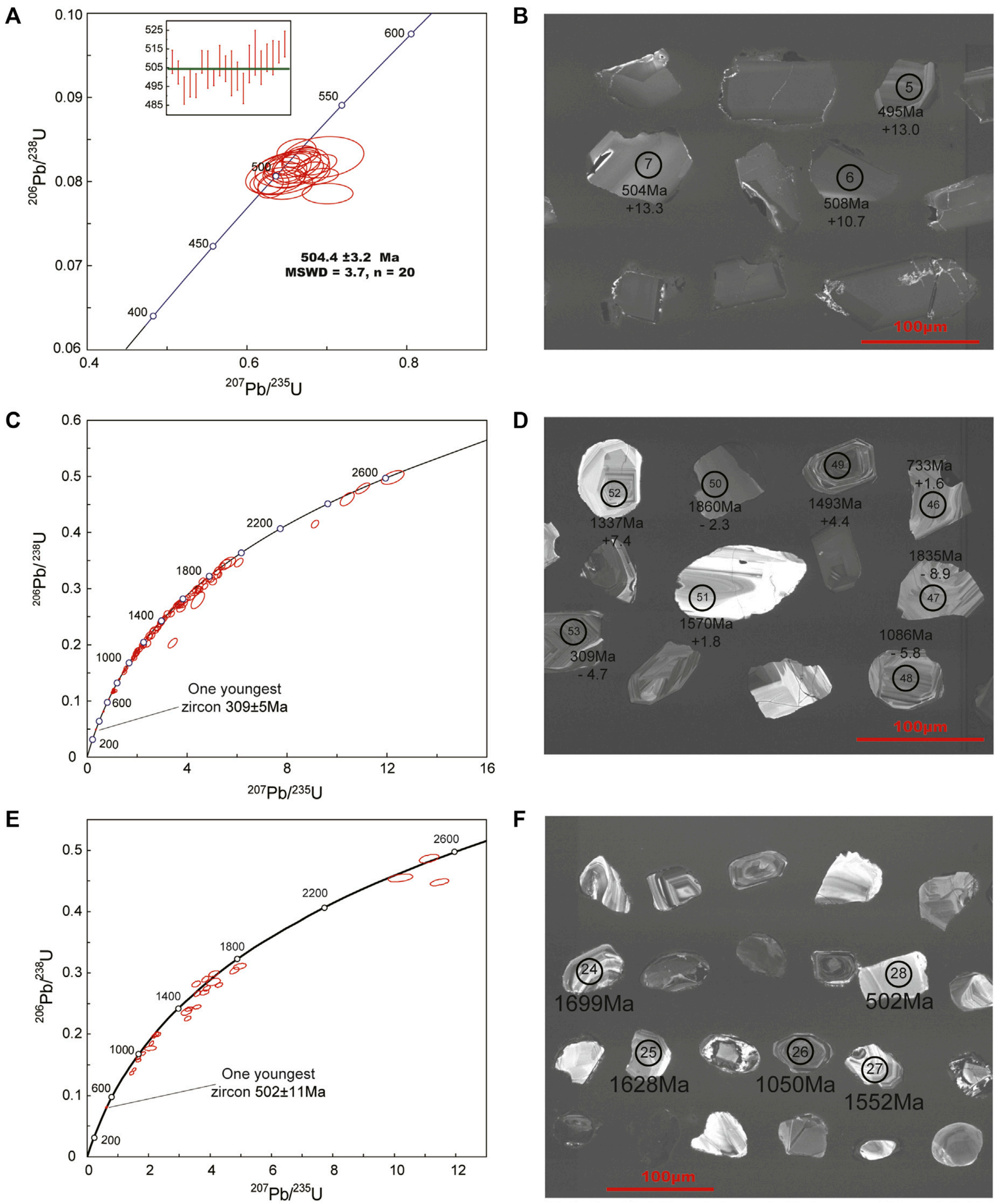

FIGURE 6 | CL images and Concordia U-Pb diagram for gabbros and sandstone of the Huaniushan complex in Beishan. **(A and B)** are LA-ICP-MS U-Pb age and CL images of gabbro (20HNS27); **(C and D)** are LA-ICP-MS U-Pb age and CL images of the sandstone in the complex (20HNS34); **(E and F)** are LA-ICP-MS U-Pb age and CL images of sandstone (20HNS15) in the northern part of the complex.

Basaltic rocks are composed of plagioclase, magnetite, ilmentite, minor olivine, and volcanic glass (dis-glass), and some samples have a little amount of clinopyroxene (**Figure 4H**).

The sandstone samples were collected in the middle (20HNS34) and northern (18HNS15) part of the Huaniushan complex (**Figures 2, 3**). These samples are well-bedded and

TABLE 4 | Sr-Nd isotopic data of basalt from the Huaniushan complex in the Beishan orogen, NW China.

Sample	age (Ga)	Rb	Sr	$^{87}Rb/^{86}Sr$	$^{87}Sr/^{86}Sr$	2s	$(^{87}Sr/^{86}Sr)_i$	Sm	Nd	$^{147}Sm/^{144}Nd$	$^{143}Nd/^{144}Nd$	2s	$(^{143}Nd/^{144}Nd)_i$	e_{Nd}
06LY10-1	0.504	83.2	85.8	0.2808	0.70591	0.000011	0.70389	2.7	9.4	0.1706	0.51314	0.000007	0.512572	11.4
06LY11-1	0.504	84.6	32.1	0.7620	0.70901	0.000011	0.70354	0.3	1.4	0.1249	0.51314	0.000012	0.512730	14.5
11HN03-1	0.504	0.8	117.6	0.0204	0.70490	0.000014	0.70475	2.0	6.0	0.2012	0.51296	0.000011	0.512294	6.0
11HN09-1	0.504	3.8	120.8	0.0901	0.70518	0.000010	0.70453	2.6	8.0	0.1961	0.51286	0.000012	0.512217	4.5
06L12-1	0.504	101.0	252.0	0.1161	0.70674	0.000018	0.70590	4.7	21.4	0.1332	0.51265	0.000011	0.512210	4.3

develop EW-trending foliations as shown in **Figure 4F**. They are mainly composed of bedded quartz and tuffs (**Figure 4I**).

ANALYTICAL METHODS

The zircon U-Pb datings were dated using a LA-ICP-MS with an ESI New Wave NWR 193UC (TwoVol2) laser ablation system connected to an Agilent 8900 Inductively Coupled Plasma Mass Spectrometry (ICPMS) at Beijing Quick-Thermo Science and Technology Co., Ltd,. Details of the procedure can be found in the study by Ji et al., (2020). *In situ* Lu–Hf isotope measurements were performed using a Thermo Finnigan Neptune-Plus MC–ICP–MS fitted with a J-100 femtosecond laser ablation system Applied Spectra Inc. housed at the Beijing Chron Technology Co., Ltd., Beijing, China. The analytical procedures and calibration methods are similar to those described by Wu et al. (2006). Zircons were ablated for 31 s at a repetition rate of 8 Hz at 16J/cm^2, and ablation pits were ~30 μm in diameter. During analysis, the isobaric interference of ^{176}Lu on ^{176}Hf was negligible due to the extremely low $^{176}Lu/^{177}Hf$ in zircon (normally <0.002). The mean $^{173}Yb/^{172}Yb$ value of individual spots was used to calculate the fractionation coefficient (β_{Yb}) and then to calculate the contribution of ^{176}Yb to ^{176}Hf. An isotopic ratio of $^{173}Yb/^{172}Yb = 1.35274$.

Major elements were determined by X-ray fluorescence spectrometry (XRF); trace elements were analyzed by inductively coupled plasma techniques (ICP) at the Geological Test and Analysis Center of the Beijing Research Institute of Uranium Geology. Details of the procedure can be found in the study by Mao et al. (2018). Sr-Nd isotopic analyses were performed in the Institute of Geology and Geophysics (IGG), Chinese Academy of Sciences, Beijing.

Isotopic compositions of Sr and Nd analyses were analyzed on a Thermo Fisher Scientific Neptune Plus MC-ICP-MS at the Institute of Geology and Geophysics, Chinese Academy of Sciences (IGGCAS) in Beijing. The measurements were carried out following the isotope dilution procedures of Yang YH et al., (2010). A static multi-collection mode was used during the measurements, and a traditional caution exchange technique was adopted for the chemical separation. The mass fractionation corrections for Sr and Nd isotopic ratios were based on $^{88}Sr/^{86}Sr = 8.375209$ and $^{146}Nd/^{144}Nd = 0.7219$.

RESULTS

The zircon U-Pb dates for the gabbro and sediment blocks are shown in **Table 1**. Major and trace element contents, zircon Hf, and Sr-Nd isotopic data are shown in **Tables 1**, **2**, **3** and **4**.

Zircon U-Pb Age and Hf Isotopes

A gabbro and two sedimentary samples from the Huaniushan complex (**Figures 3**, **6**) were analyzed. All the U-Pb and Hf isotopic data are shown in **Tables 1** and **2**.

Gabbro

The zircon grains from the granite sample 20HNS27 show length/width ratios of 1.2–2 with size ranging from 50 to 120 μm. They are euhedral and transparent and show clear magmatic oscillatory zoning in CL images (**Figure 6B**). The Th/U ratios of analyzed zircons range from 0.92–2.91 and are consistent with a magmatic origin (Hoskin and Schaltegger, 2003). The 20 analyses give concordant $^{206}Pb/^{238}U$ ages ranging from 493 to 518 Ma, with a weighted mean age of 504.4 ± 3.2 Ma (MSWD = 3.7; **Figure 6A**). The age records the crystallization time for the gabbro block. Lu-Hf isotopic analyses of the gabbro yielded $^{176}Hf/^{177}Hf$ values of 0.282691–283097 and high $\varepsilon_{Hf}(t)$ values (+8.07 to +17.74) (**Figure 7**).

Clastic Sediments

A total of 118 analyses of zircon grains from two sedimentary samples (20YY34 and 18HNS15) from the Huaniushan complex (**Figure 6**) yielded 116 concordant ages [concordance % > 90% or <110%, the age <1,500 Ma used U/Pb age, and the age >1,500 Ma used Pb/Pb age (Spencer et al., 2016)]. Only concordant ages are described and discussed below.

Zircons from sample 20HNS34 are weak rounded structures and are 50–100 μm long with length/width ratios of 1.0–1.5. They have prominent zones in CL images (**Figure 6D**). They have variable Th/U values of 0.04–1.88. The 89 analyzed zircon grains yield concordant ages ranging from 309 ± 5 Ma to 2,657 ± 29 Ma. The youngest zircon yields concordant Pb^{206}/U^{238} age of 309 ± 8 Ma (**Figures 6C**, **12A**). Eighty-one zircon grains (91% of the total) have concordant age of 703 Ma to 1903 Ma, and show three peaks at 706 Ma, 1,093 Ma, and 1880 Ma. Five grains are older than 2033 Ma, scattered ages at 2,468 Ma (**Figures 6C**, **12A**). The youngest zircon age (309 Ma) is interpreted as the MDA of the sandstone. Lu-Hf isotopic analyses of the detrital zircons yielded $\varepsilon_{Hf}(t)$ values ranging from −11.7 to +10.5 (**Figure 7**).

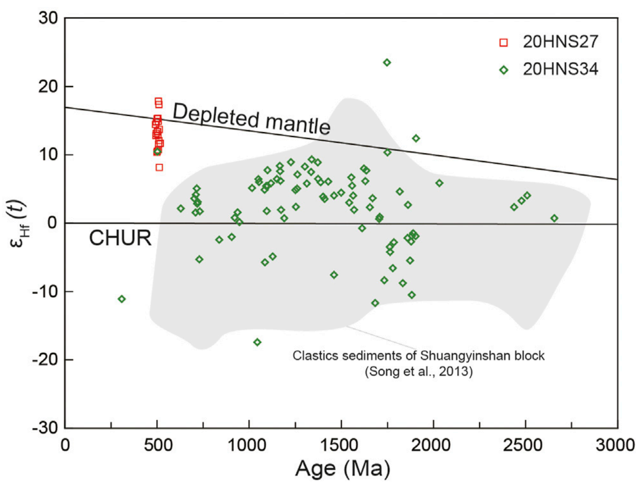

FIGURE 7 | $\varepsilon_{Hf}(t)$ vs. age diagram for the Huaniushan complex in the Beishan orogen. The Hf isotope data of the sediments from the Heiyingshan block are after (Song et al., 2013).

Zircons from sample 18HNS15 are weak rounded structures too. They are 50–90 μm long, with length/width ratios of 1.0–1.5 and have prominent zones in CL images (**Figure 6F**). They have variable Th/U values of 0.19–1.36. Of 28 analyzed zircon grains, 27 zircon grains yield concordant ages ranging from 501 ± 5 Ma to 2,703 ± 28 Ma (**Figures 6E**, **12B**). Twenty-three zircon grains (85% of the total) have concordant age range from 824 Ma to 1818 Ma and show four peaks at 840 Ma, 1,168 Ma, 1,680 Ma, and 1876 Ma. Three grains show age of 2,481–2,703 Ma (**Figure 12B**). The youngest zircon yields concordant Pb^{206}/U^{238} age of 501 ± 5 Ma (**Figures 6E**, **12B**). This age is interpreted as the MDA of the sandstone.

Whole-Rock Geochemistry

Whole-rock major, trace elements, and Sr-Nd isotope data of the basalts and gabbros are listed in **Tables 3** and **4**.

Basalt

The basalts can be separated into MORB and OIB types according to their element contents.

The major element compositions of the MORB-type basalts and gabbros have variable contents of SiO_2 (44.08–51.22 wt%), TiO_2 (0.55–1.45 wt%), Al_2O_3 (11.43–15.01 wt%), MgO (6.25–18.17 wt%), and CaO (8.83–13.98 wt%). They are classified as tholeiitic basalts (**Figure 8**). These basalts exhibit high Cr (104–1,303 ppm) and Ni (71–649 ppm) concentrations. Their depleted to slightly enriched REE patterns (**Figure 9A**) are like those of MORBs, with $(La/Yb)_N$ ratios of 0.68–1.53 and slightly negative to positive Eu anomalies (δEu = 0.90–1.38) (**Figure 9A**). On the primitive mantle–normalized spider diagrams (**Figure 9B**), they have a positive Rb, Ba anomalies, and negative to positive Sr anomalies. Four basaltic samples have relatively low $(^{87}Sr/^{86}Sr)_i$ values of 0.70354–0.70475, and high $\varepsilon_{Nd}(t)$ values of +4.5 to +14.5 (**Figure 10**).

Two OIB-type basaltic samples have contents of SiO_2 (46.97–46.99 wt%), TiO_2 (2.48–2.56 wt%), Al_2O_3 (8.59–9.06 wt %), CaO (10.51–10.74 wt%), and MgO (10.91–12.67 wt%), and relatively high Cr (656–828 ppm) and Ni (447–532 ppm). They are tholeiitic basalts (**Figure 8**). They are enriched in LREE and comparable to those of OIB with $(La/Yb)_N$ ratios between 7.13 and 7.17 on the REE pattern diagram (**Figure 9C**). They have positive Nb and Ti anomalies and negative Sr anomalies on the primitive mantle–normalized spider diagrams (**Figure 9D**). One sample has the highest $(^{87}Sr/^{86}Sr)_i$ value of 0.70590 and the lowest $\varepsilon_{Nd}(t)$ value of +4.3 (**Figure 10**).

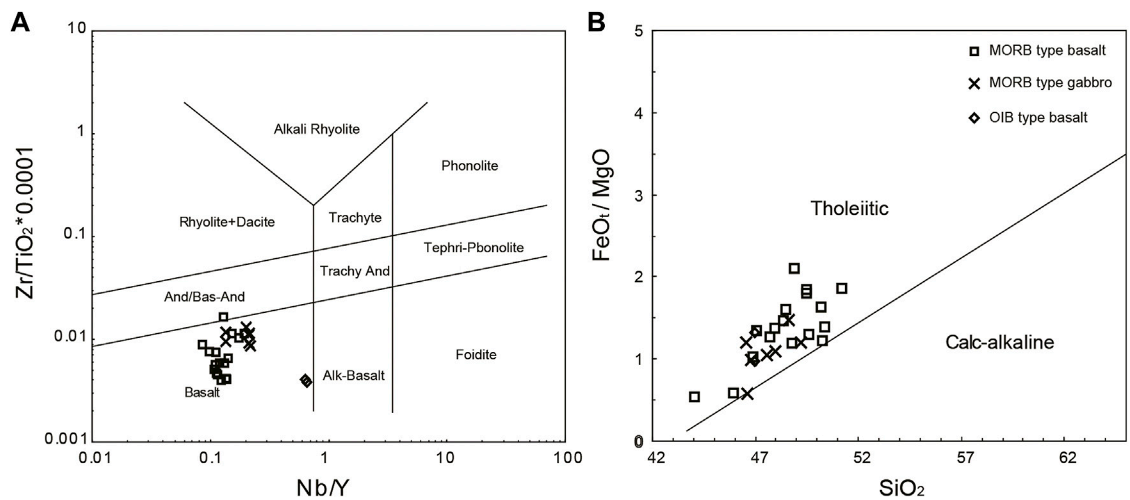

FIGURE 8 | Geochemical classification diagrams of the Huaniushan complex in the Beishan orogen, NW China. **(A)** Zr/Ti vs. Nb/Y diagram (Winchester and Floyd, 1977) and **(B)** FeO_t/MgO vs. SiO_2 diagram (Myashiro, 1974).

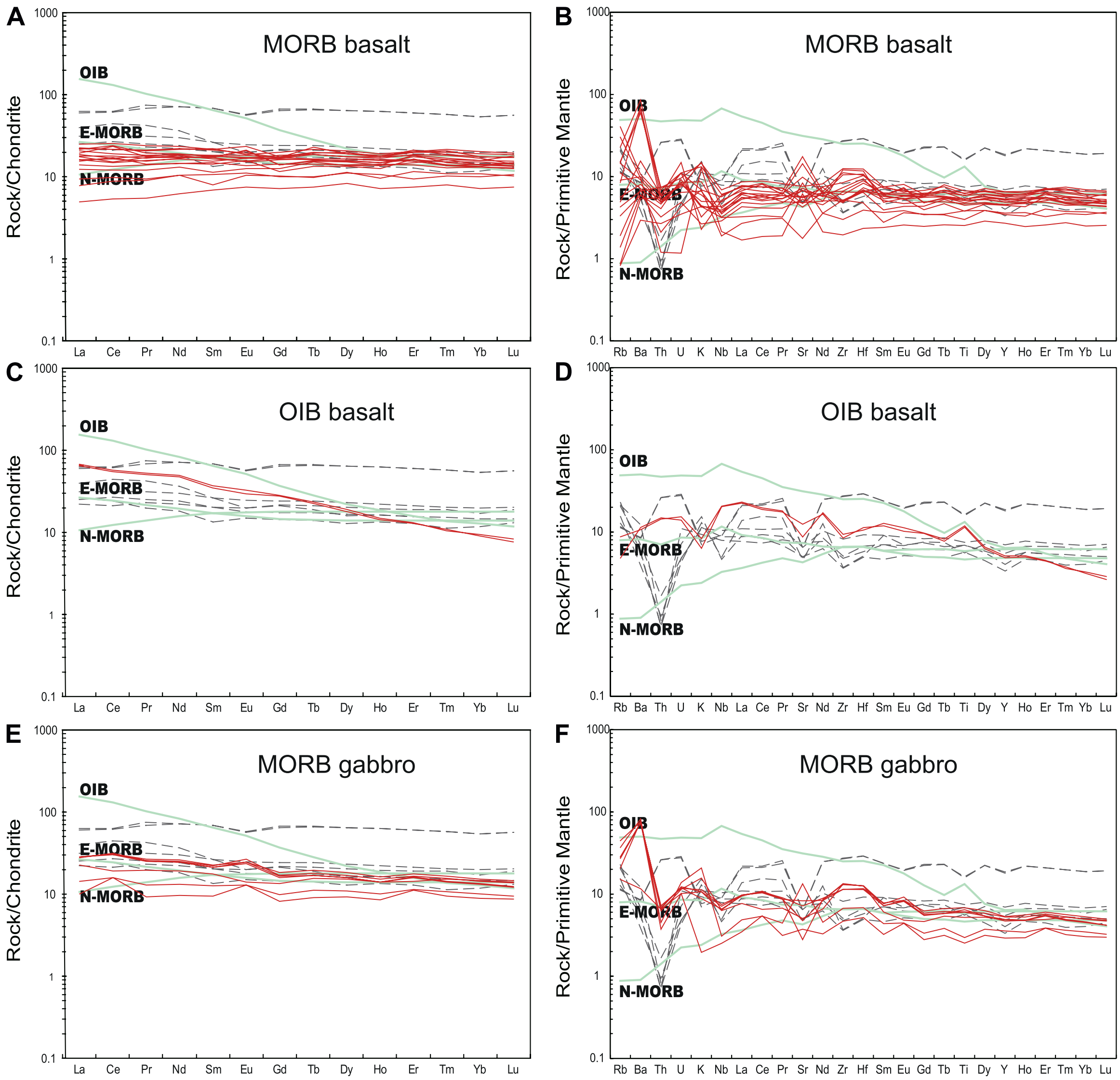

FIGURE 9 | Chondrite-normalized REE patterns and Primitive Mantle (PM)–normalized multi-element diagrams for the gabbros from the Huaniushan complex. The chondrite values are given by Boynton, (1984). The PM, N-MORB, E-MORB, and OIB values are given by Sun and McDonough, (1989). Data of dash lines for the Gubaoquan eclogite are given by Qu et al., (2011).

Gabbro

The gabbroic rocks have similar geochemical compositions to the MORB-type basalts. They are tholeiitic basalts (**Figure 8**) and have narrow contents of SiO_2 (46.57–49.19 wt %), but wide range of TiO_2 (0.55–1.47 wt%), Al_2O_3 (10.46–17.83 wt%), CaO (8.40–12.14 wt%), and MgO (6.84–16.95 wt%), and high contents of Cr (143–1,535 ppm) and Ni (72–623 ppm). They have slightly enriched REE patterns ($(La/Yb)_N$ =(1.15–2.17) and positive Eu anomalies (δEu = 0.90–1.46, **Figure 9E**). They are enriched in Rb and Ba and have slightly negative to positive Sr and Ti anomalies on the primitive mantle–normalized spider diagrams (**Figure 9F**). The $^{176}Hf/^{177}Hf$ ratios of these zircons for the gabbros range from 0.281973 to 0.283097, and the high positive ε_{Hf} *(t)* values range from +8.2 to +17.8 (**Figure 7**).

DISCUSSION

Age of the Liuyuan Accretionary Complex

Huaniushan Complex

The zircon U-Pb dates reveal the crystallization time for the gabbro block to be 504.4 ± 3.2 Ma (**Figure 6A**), suggesting that the Huaniushan complex contains the Cambrian oceanic fragments. Yang J. G. et al. (2010) reported that basalts of the Huaniushan complex yielded zircon U-Pb age of 1,071 ± 5 Ma.

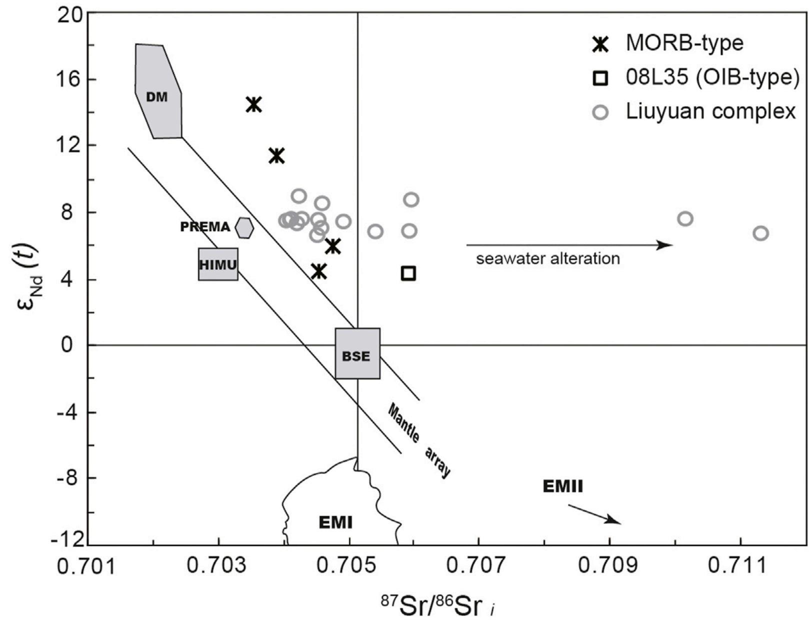

FIGURE 10 | $\varepsilon_{Nd}(t)$ vs. initial ($^{87}Sr/^{86}Sr)_i$ (Ma) diagram for the Huaniushan complex in Beishan orogen. DM, Depleted mantle; BSE, Bulk silicate earth; EMI and EMII, enriched mantle; HIMU, mantle with high U/Pb ratio; PREMA (Zindler and Hart, 1986). The Sr-Nd isotope data of the Liuyuan complex are after (Mao et al., 2012b).

Thus, available data indicate that the ophiolitic blocks contain Cambrian to Proterozoic oceanic fragments.

Several methods are used for calculating the MDA of sedimentary rocks from their detrital zircon U-Pb ages (Coutts et al., 2019). Here, we use the youngest grain with a 2σ uncertainty. The sandstone samples (20YY34 and 18HNS15) yield minimum ages of 309 ± 5 Ma and 501 ± 5 Ma, respectively (**Figures 6C,E**). Thus, the MDA of the sandstone 20YY34 is less than 309 ± 5 Ma, while the MDA of the sandstone 18HNS15 is less than 501 Ma. The least MDA of the sandstone matrix of the Huaniushan complex belt deposit in the tholeiitic Carboniferous, which have younger ophiolite fragments (504 Ma), indicates that the northward subduction beneath the Huaniushan arc may have started at least at ca. 501 Ma, and final accretion of the Huaniushan ophiolitic mélange was after the tholeiitic Carboniferous (309 Ma). Thus, the geochronological studies reveal the blocks of the Huaniushan complex age ranging from 309 Ma to 1,071 Ma.

Liuyuan Accretionary Complex

Numerous ophiolite fragments have been reported in the Liuyuan accretionary complex at the southern margin of the Huaniushan arc (**Figure 1B** and **Table 5**). The zircon U-Pb dates reveal that the age of the ophiolite blocks of the Liuyuan accretionary complex is from 1,071 Ma to 270 Ma (**Table 5**), e.g. 1) the basalts and gabbros of the Huaniushan ophiolitic complex have ages of 1,071 ± 5 Ma and 504 ± 3 Ma [(Yang J. G. et al., 2010); this study], respectively; 2) the Gubaoquan eclogites have protolith ages of 819 Ma to 1,007 Ma (Yang et al., 2006; Liu et al., 2011; Qu et al., 2011; Saktura et al., 2017); 3) the gabbro of the Huitongshan ophiolite has an age of 446 ± 3 Ma (Yu et al., 2012); 4) the gabbro of the Zhangfangshan ophiolite has an age of 363 ± 4 Ma (Yu et al., 2012); 5) gabbros of the Liuyuan ophiolite have an age of 270–286 Ma (Mao et al., 2012b; Zheng et al., 2014; Wang et al., 2016); 6) the gabbro of the Yinaoxia ophiolite has an age of 281 ± 11 Ma (Zheng et al., 2014). The detrital zircon LA-ICPMS U-Pb dates for these sediments and metamorphic sediments blocks revealed that the minimum age of clastic sediments blocks is from 457 Ma to 234 Ma (Wang et al., 2016; Tian and Xiao, 2020; this study).

In summary, the geochronological studies suggest the Liuyuan accretionary complex are composed of Neoproterozoic to late Triassic oceanic crust and sedimentary fragments. The Liuyuan Ocean may have been the latest closed branch of the Paleo-Asian Ocean.

Tectonic Setting of the Huaniushan Complex

The Huaniushan complex has been thrust-imbricated on the Ordovician volcanic sediments in the northern part of the Liuyuan accretionary complex. They display block-in-matrix structures and are intruded by the late Triassic Huaniushan A-type granite (Li et al., 2012). Different degree schists and cleaved fragments in the complex consist of ultramafic rocks, gabbros, basalts, cherts, limestones, and sandstones which are enclosed in a matrix of chlorite–phyllite strong schist and cleaved sandstone (**Figures 4**, **5**). Ordovician sediments

TABLE 5 | Regional age data for the Liuyuan accretionary complex.

Number	Sample no.	Locations	Rock type	Analyzed minerals	Analysis method	Ages with errors (Ma)	References
1. Liuyuan accretionary complex							
			Huaniushan melange				
1	20YY27	Huaniushan	Gabbro	Zircon	LA-ICPMS	504 ± 3	this study
2	07Bj1C	Huaniushan	Basalt	Zircon	LA-ICPMS	1,071 ± 5	Yang J. G. et al. (2010)
3	20HNS34	Huaniushan	Sandstone	Zircon	LA-ICPMS	309 ± 5 (1), 629 ± 8(1), 703–1903 (81), 2,468 ± 11 (4)	this study
4	18HNS15	Huaniushan	Sandstone	Zircon	LA-ICPMS	502 ± 5 (1), 503 ± 8(1),824–1818 (23), 2,500(3)	
			Gubaoquan eclogite				
5	04Y18-6	Gubaoquan	Eclogite	Zircon	SHRIMP	439 ± 10 (1 rim), 819 ± 20 (13 core), 1,007 ± 20 (2 core)	Yang et al. (2006)
6		Gubaoquan	Eclogite	Zircon		467 ± 16 (1 rim), 881 ± 12 (1 core)	Qu et al. (2011)
7	B101-15	Gubaoquan	Eclogite	Zircon	LA-ICPMS	464 ± 11 (7 rim), 889 ± 5 (17 core)	Liu et al. (2011)
8	B101-14	Gubaoquan	Eclogite	Zircon	LA-ICPMS	468 ± 11 (1 rim), 880 ± 7 (14 core)	Liu et al. (2011)
9	14GBQ1	Gubaoquan	Eclogite	Zircon	SHRIMP	466 ± 27 (rims), 860 ± 18 (core)	Saktura et al. (2017)
10	14GBQ2	Gubaoquan	augen orthogneiss	Zircon	SHRIMP	920 ± 14	Saktura et al. (2017)
			Huitongshan ophiolite				
11	BS103	Huitongshan	Gabbro	Zircon	LA-ICPMS	446.1 ± 3.0	Yu et al. (2012)
			Zhangfangshan ophiolite				
12	BS090	Zhangfangshan	Gabbro	Zircon	LA-ICPMS	362.6 ± 4.0	Yu et al. (2012)
			Liuyuan melange				
13	DQ43	S Liuyuan on highway	Gabbro	Zircon	LA-ICPMS	286 ± 2	Mao et al., 2012b
14	LY-41	S Liuyuan on highway	Gabbro	Zircon	LA-ICPMS	270 ± 1	Wang et al. (2016)
15	LY-108	W Liuyuan on highway	Gabbro	Zircon	LA-ICPMS	280 ± 6	Wang et al. (2016)
16	LY-122	E Liuyuan on highway	Gabbro	Zircon	LA-ICPMS	277 ± 3	Wang et al. (2016)
17	LY25	S Liuyuan on highway	Black sandstone	Zircon	LA-ICPMS	234 ± 10, 281 ± 11, 438 ± 19	Wang et al. (2016)
18	LY20	S Liuyuan on highway	Volcanic clastics (in the pillow lava)	Zircon	LA-ICPMS	268 ± 9, 429 ± 17	Wang et al. (2016)
19	LY92	S Liuyuan on highway	Sandstone	Zircon	LA-ICPMS	285 ± 5, 442 ± 5	Wang et al. (2016)
20	LY89	NE Xiadong	Dacite	Zircon	LA-ICPMS	279 ± 3, 438 ± 10	Wang et al. (2016)
21	LY88	NE Xiadong	Dacite	Zircon	LA-ICPMS	280 ± 4, 424 ± 19	Wang et al. (2016)
22	LY95	NE Xiadong	Rhyolite	Zircon	LA-ICPMS	277 ± 4	Wang et al. (2016)
			Yinaoxia ophiolte				
23	Y-5	W Yinaoxia	Gabbro	Zircon	SHRIMP	281 ± 11	Zheng et al. (2014)
			Clastic sediments in the Liuyuan accretionary complex				
24	LY45	E Gubaoquan	Mylonite	Zircon	LA-ICPMS	926 ± 15	Wang et al. (2016)
25	LY-59	N Liuyuan on highway	Sandstone	Zircon	LA-ICPMS	293 ± 5, 440 ± 6	Wang et al. (2016)
26	LY-74	E Gubaoquan	O-S schist	Zircon	LA-ICPMS	457 ± 33	Wang et al. (2016)
			2. Shuangyinshan–Huaniushan arc				
27	LY101	E Gubaoquan	Granite	Zircon	LA-ICPMS	445 ± 4	Wang et al. (2016)

(Continued on following page)

TABLE 5 | (*Continued*) Regional age data for the Liuyuan accretionary complex.

Number	Sample no.	Locations	Rock type	Analyzed minerals	Analysis method	Ages with errors (Ma)	References
28	LY-94	NE Xiadong	Granite	Zircon	LA-ICPMS	422 ± 5	Wang et al. (2016)
29	LY-65	E Gubaoquan	Mylonitized diorite	Zircon	LA-ICPMS	466 ± 7	Wang et al. (2016)
30	LY-69	E Gubaoquan	Granite	Zircon	LA-ICPMS	451 ± 6	Wang et al. (2016)
31	LY-75	E Gubaoquan	Granitic lens	Zircon	LA-ICPMS	895 ± 15	Wang et al. (2016)
33	LYB19	E Huitongshan	Adakitic granite	Zircon	LA-ICPMS	424 ± 4	Mao et al., 2012a
34	08LY01	N Liuyuan	Arc dacite	Zircon	LA-ICPMS	442 ± 3	Mao et al., 2012a
35	08LY02	N Liuyuan	Nb-enriched basalts	Zircon	LA-ICPMS	451 ± 4	Mao et al., 2012a
36	08 L05	N Liuyuan	Adakitic granite	Zircon	LA-ICPMS	374 ± 3	Mao et al., 2012a
37	B70823-8	W Huitongshan	K-feldspar granites	Zircon	LA-ICPMS	397 ± 3	Li et al. (2011)
38	09dds45-1	Dundunshan	Rhyolites	Zircon	LA-ICPMS	369 ± 3	Guo et al. (2014)
39	09DDS41-1	Dundunshan	Syenoporphyry	Zircon	LA-ICPMS	371 ± 1	Guo et al. (2014)
40		Liuyuan	Granodiorite	Zircon	SHRIMP	423 ± 8	Zhao et al. (2007)
41		Liuyuan	Monzogranite	Zircon	SHRIMP	397 ± 7	Zhao et al. (2007)
42	HT	Liuyuan	Potassium granite	Zircon	SHRIMP	436 ± 9	Zhao et al. (2007)
43	SF07	N Huaniushan	A-type granite	Zircon	LA-ICPMS	415 ± 3	Li et al. (2009)
44		Heishan	Gabbro of Heishan Alaska ultramafic–mafic complex	Zircon	LA-ICPMS	375 ± 5	Xie et al. (2012)
45		Dashantou	Gabbro of Dashantou Alaska ultramafic–mafic complex	Zircon	LA-ICPMS	374 ± 3	Wang et al. (2015)
46		Guishishan	Gabbro of Guishishan Alaska ultramafic-mafic complex	Zircon	LA-ICPMS	359 ± 4	Yang et al. (2016)
47		Miaomiaojin	Gabbro of Miaomiaojin Alaska ultramafic–mafic complex	Zircon	LA-ICPMS	378 ± 5	Duan et al. (2021)
48	B70817–2.1	Dahuoluo	Dahuoluo monzonite	Zircon	LA-ICPMS	238 ± 1	Li et al. (2012)
49	B70817–2.3	Dahuoluo	Dahuoluo Granodiorite	Zircon	LA-ICPMS	240 ± 3	Li et al. (2012)
50	B8062-6	Daquan	Syenite	Zircon	LA-ICPMS	221 ± 2	Li et al. (2012)
51	DQ09819-8	Daquan	Syenite	Zircon	LA-ICPMS	225 ± 1	Li et al. (2012)
52	B70822-4	Huaniushan	Syenogranite	Zircon	LA-ICPMS	221 ± 3	Li et al. (2012)
53	HNS09823–2.2	Huaniushan	Granite porphyry	Zircon	LA-ICPMS	217 ± 2	Li et al. (2012)
54	B80628-3	Changliushui	Syenogranite	Zircon	LA-ICPMS	222 ± 2	Li et al. (2012)
55	MSD09821	Baixianishan	Monzogranite	Zircon	LA-ICPMS	224 ± 1	Li et al. (2012)
56		S Huaniushan	Meta-dacite	Zircon	LA-ICPMS	455 ± 1	Xie et al. (2018)
			3. Shibanshan accretionary arc				
58	LY-76	Xiaodong	Sandstone (Xiadong)	Zircon	LA-ICPMS	285 ± 5, 433 ± 7	Wang et al. (2016)
59	LY-77	Xiaodong	Lam (dyke) (Xiadong)	Zircon	LA-ICPMS	227 ± 7	Wang et al. (2016)
60	LY56	S Gubaoquan	*Sandstone*	Zircon	LA-ICPMS	284 ± 7, 429 ± 24	Wang et al. (2016)
61	14SBD06	Xiaodong	Gneissic granitoid	Zircon	LA-ICPMS	305 ± 2	Song et al. (2016)
62	14SBD04	Xiaodong	Gneissic granitoid	Zircon	LA-ICPMS	294 ± 2	Song et al. (2016)
63	14BDZ12	Baidunzi	Quartzite	Zircon	LA-ICPMS	299 ± 3, 299–986	Song et al. (2016)
64	BS03-4	Yinaoxia	Gabbroic dikes	Zircon	LA-ICPMS	267 ± 3	Zheng et al. (2020)
65	BS03-6	Yinaoxia	High-Mg dioritic dikes	Zircon	LA-ICPMS	270 ± 2	Zheng et al. (2020)
66	BS03-5	Yinaoxia	Granites	Zircon	LA-ICPMS	280 ± 3	Zheng et al. (2020)
67	BS03-10	Yinaoxia	Granites	Zircon	LA-ICPMS	280 ± 3	Zheng et al. (2020)
68	BS05-1	Yinaoxia	Granites	Zircon	LA-ICPMS	277 ± 3	Zheng et al. (2020)
69	BS07-75	Yinaoxia	Biotite granite	Zircon	LA-ICPMS	282 ± 3	Zhang et al. (2011)
70	BS47-2	Xiaoxigong	Adakitic granites	Zircon	LA-ICPMS	268 ± 3	Zheng et al. (2020)
71	BS47-6	Xiaoxigong	Adakitic granites	Zircon	LA-ICPMS	269 ± 2	Zheng et al. (2020)
72	DJQ11-9	Xiaoxigong	Adakitic granites	Zircon	LA-ICPMS	267 ± 1	Zheng et al. (2020)
73	FS-7	Yinaoxia	Rhyolite	Zircon	LA-ICPMS	273 ± 1	Zheng et al. (2016)
74		Yinaoxia	Monzonitic granite	Zircon	LA-ICPMS	266 ± 2	Zhang et al. (2010)

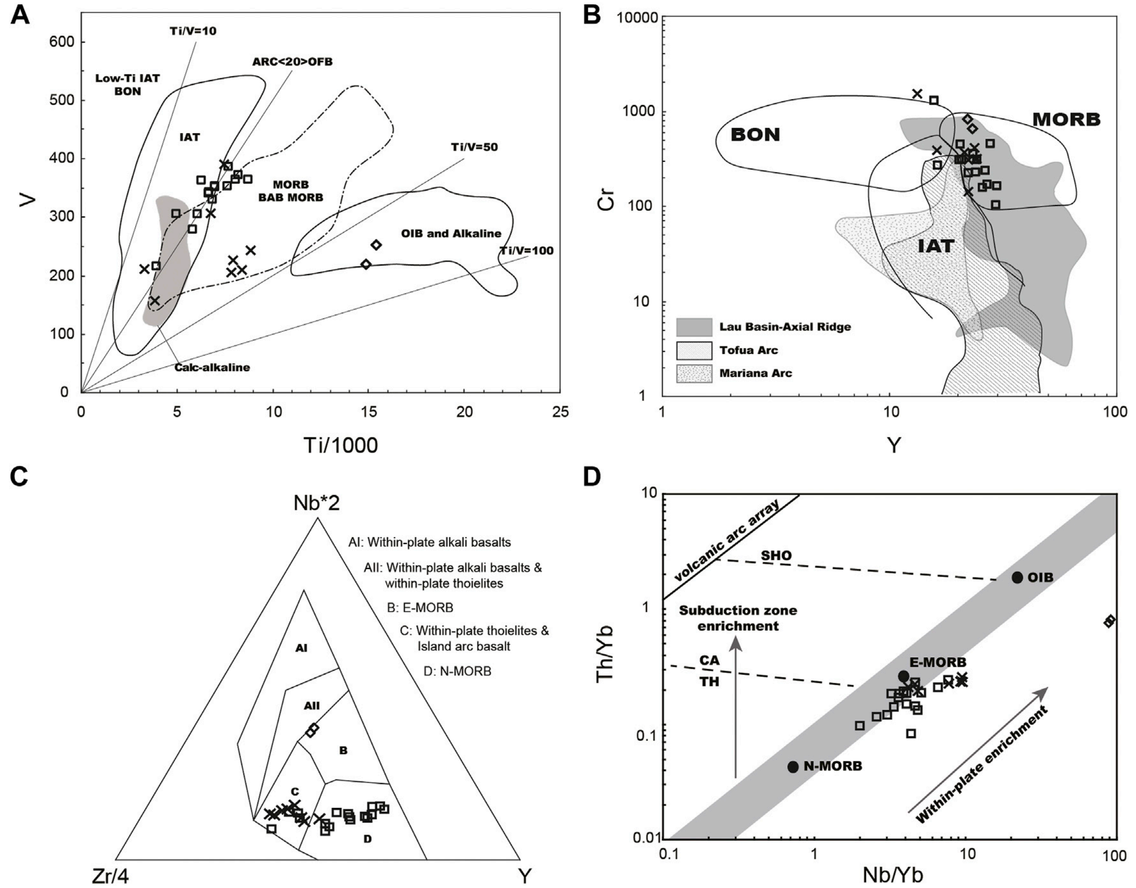

FIGURE 11 | (A) Ti vs. V discrimination diagram for the rocks from the Huaniushan complex (Shervais, 1982). **(B)** Cr vs. Y discrimination diagram for the rocks from the Huaniushan complex, after (Pearce et al., 1981), BON-boninite, IAT-island arc tholeiite, and MORB-mid-oceanic ridge. The fields of the Lau Basin-Axial Ridge, the Tofua Arc, Mariana Trough and Mariana Arc are after (Hawkins, 2003). **(C)** Nb-Zr-Y discriminant diagrams (Meschede, 1986) and **(D)** Th/Yb vs. Nb/Yb discriminant diagram [SHO: shoshonite, CA-Calc: alkaline, TH: tholeiite (Pearce, 2008)]. Symbols are the same as those in **Figure 6**.

developed sub-vertical tight folds, the axes of which strike east–west. All these structures indicate that the Huaniushan complex underwent intense top-to-the-south thrusting and east–west shearing. Although most of the different rock types in the Huaniushan complex are mutually juxtaposed by thrusts, the blocks of basalt, gabbro, serpentinized ultramafic, limestone, and chert with tuff beds are probably fragments of oceanic plate stratigraphy. They would have provided information on the travel history of the oceanic plate from ridge to trench (Kusky et al., 2013). All the mafic blocks in the Huaniushan complex are tholeiitic magma, but as described above, they consist of MORB- and OIB-type geochemical signatures.

The MORB-type basalts and gabbros have slightly depleted to enriched LREE patterns (La/Yb_N = 0.68–1.53, **Figures 9A,E**), as also are the similar trace element patterns with their positive Ba and negative to positive Rb and Sr anomalies (**Figures 9B,F**). Their enrichments in fluid-soluble elements (Rb and Ba) and Sr-Nd isotope plot above the mantle array indicate seawater alteration (Hawkins, 2003; Reagan et al., 2010) (**Figure 10**). On Ti-V and Cr-Y diagrams, most of the mafic rocks plot in the field of MORB (**Figures 11A,B**). And, they further plot as MORB and within-plate tholeiites on the Nb-Zr-Y diagram (**Figure 11C**), and close to the E-MORB basalt field on the Th/Yb-Nb/Yb diagram (**Figure 11D**). Their $\varepsilon_{Nd}(t)$ values have relatively high and wide range changes (+4.5 to +14.5) and can be subdivided into two groups. Group 1 has higher $\varepsilon_{Nd}(t)$ values (+11.2 to +14.5) which are more depleted than the MORB-type rocks of the Liuyuan ophiolite (+6.6 to +9.0) and the Gubaoquan eclogite (+6.3 to +6.4) (Qu et al., 2011; Mao et al., 2012b). Group 2 has relatively low $\varepsilon_{Nd}(t)$ values (+4.5- +6.0) which are lower than those of the MORB-type rocks of the Liuyuan ophiolite and Gubaoquan eclogite, but higher than those of the E-MORB–type rocks of the Gubaoquan eclogite (−1.6 to −0.1). The gabbro blocks have high $\varepsilon_{Nf}(t)$ values (+8.2–+17.8). These geochemical and isotopic features suggest that the basalts of the Huaniushan complex blocks contain MORB- and E-MORB–type basalts which are derived from the depleted to relatively enriched mantle.

The OIB-type basalts have high contents of TiO_2 (2.48–2.56 wt %), MgO (10.91–12.67 wt%), and ΣREE (99–103 ppm). Their

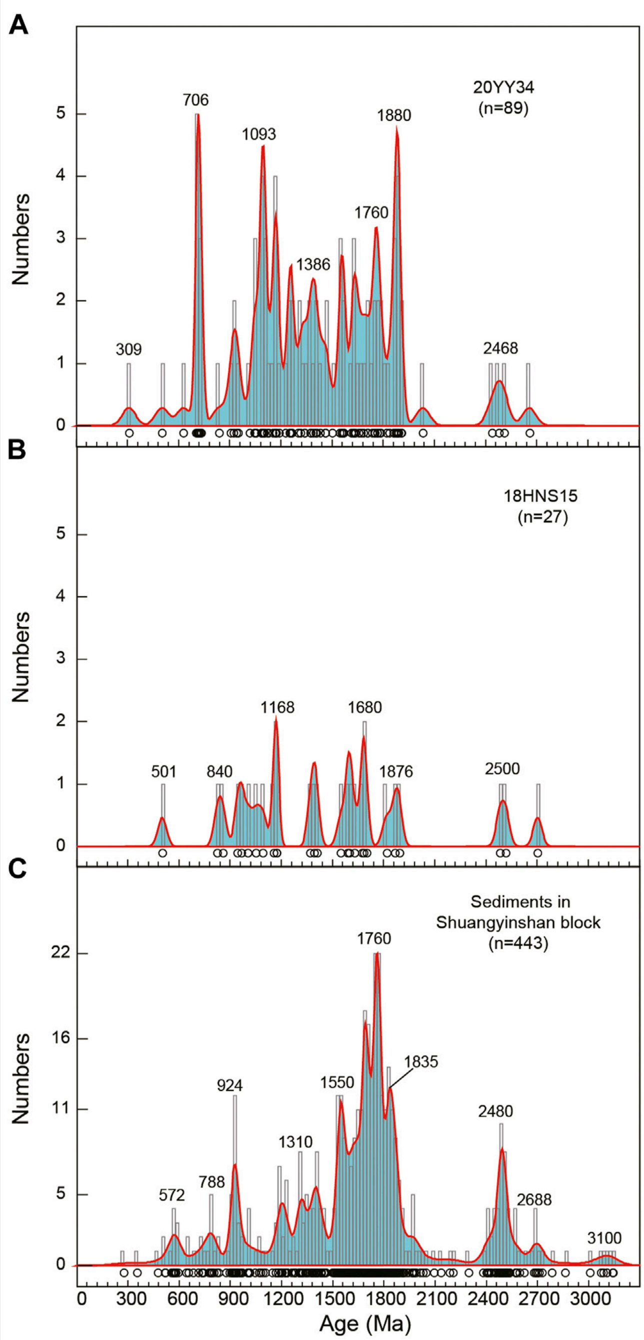

FIGURE 12 | Comparison of probability plots for zircon U-Pb ages of sedimentary rocks. **(A and B)** are from the sedimentary rocks of the Huaniushan complex in the Beishan orogen, **(C)** is from the metasedimentary rocks of Shuangyinshan block in the Beishan orogen (Song et al., 2013; Ao et al., 2016; Song et al., 2016).

REE patterns and trace element patterns plot between the MORB and OIB lines on the chondrite-normalized REE diagrams (**Figure 9C**). They have relatively lower Nd isotopic value (+4.3) than the MORB-type rocks (**Figure 10**), suggesting relatively enriched mantle sources.

All these geochemical features demonstrate that these mafic blocks in the Huaniushan complex containing the MORB-, E-MORB-, and OIB-type oceanic crust fragments, which have similar REE and trace patterns to the Gubaoquan eclogite (**Figures 9**, **11**), were probably generated in an oceanic plateau/seamount. These results are consistent with the geological fact that they consist of gabbros, basalts, cherts, and limestones. Combined with the regional data, our results and the 1,071–866 Ma MORB and E-MORB–type ocean slab metamorphic genetic Gubaoquan eclogite (Qu et al., 2011) suggest a hot spot in the Liuyuan oceanic from 1,071 Ma to 466 Ma.

Provenance of the Sediment Matrix of the Huaniushan Complex

The Huaniushan complex is located in the northernmost part of the Liuyuan accretionary complex which is situated between the Shuangyingshan–Huaniushan arc in the north and the Shibanshan arc in the south (**Figure 1B**). Therefore, the Shuangyingshan–Huaniushan arc was the main potential provenance for the sandstone matrix of the Huaniushan complex.

The two sandstones (18HNS15 and 20HNS 34) have similar and consistent detrital zircon U-Pb age populations (**Figures 12A,B**) with dominant age peaks in the period 820–1900 Ma (more than 85% of total concordant ages for each sample), and a second peak at 2,500 Ma. This age spectrum of these detrital zircons for the sedimentary blocks is similar to that of the sediments in the Shuangyinshan–Huaniushan arc (**Figure 12C**) (Song et al., 2013; Ao et al., 2016). Lu-Hf isotopic analyses of these detrital zircons yielded $\varepsilon_{Hf}(t)$ values ranging from −11.7 to +10.5 (**Figure 7**), which are plotted in the same area to the sediments in the Shuangyinshan–Huaniushan arc (Song et al., 2013). In summary, our detrital zircon LA-ICPMS U-Pb dates and Lu-Hf isotopic analyses for the sandstone blocks of the Huaniushan complex indicate that they are mainly sourced from the Precambrian blocks. Our detrital zircon LA-ICPMS U-Pb dates also find a few Paleozoic zircon grains, suggesting the young sources. As described before, the Shuangyinshan–Huaniushan arc is a Japanese type island arc. Large volume of granitoids and volcanic rocks was formed by the Liuyuan ocean subduction in the Paleozoic to Neoproterozoic to Triassic [673 Ma–217 Ma (Nie et al., 2002a; Nie et al., 2002b; Zhao et al., 2007; Mao et al., 2012a; Li et al., 2012; Wang et al., 2016); **Table 5**]. Thus, the Carboniferous to Cambrian zircon grains maybe sourced from these magmas. Both the detrital zircon age spectra and $\varepsilon_{Hf}(t)$ values are comparable with the sedimentary and magmatic record in the Shuangyinshan–Huaniushan arc. The sedimentary samples (20HNS15 and 34) were probably derived from the Shuangyinshan–Huaniushan arc in the north, further to constrain the Huaniushan complex probably formed in the forearc of the Shuangyinshan–Huaniushan arc.

Tectonic Evolution of the Liuyuan Ocean

The Liuyuan accretionary complex is very essential to understand the evolution of the Paleo-Asian Ocean and the accretionary orogenic processes of the southern Altaids (Zuo et al., 1991; Xiao et al., 2010;

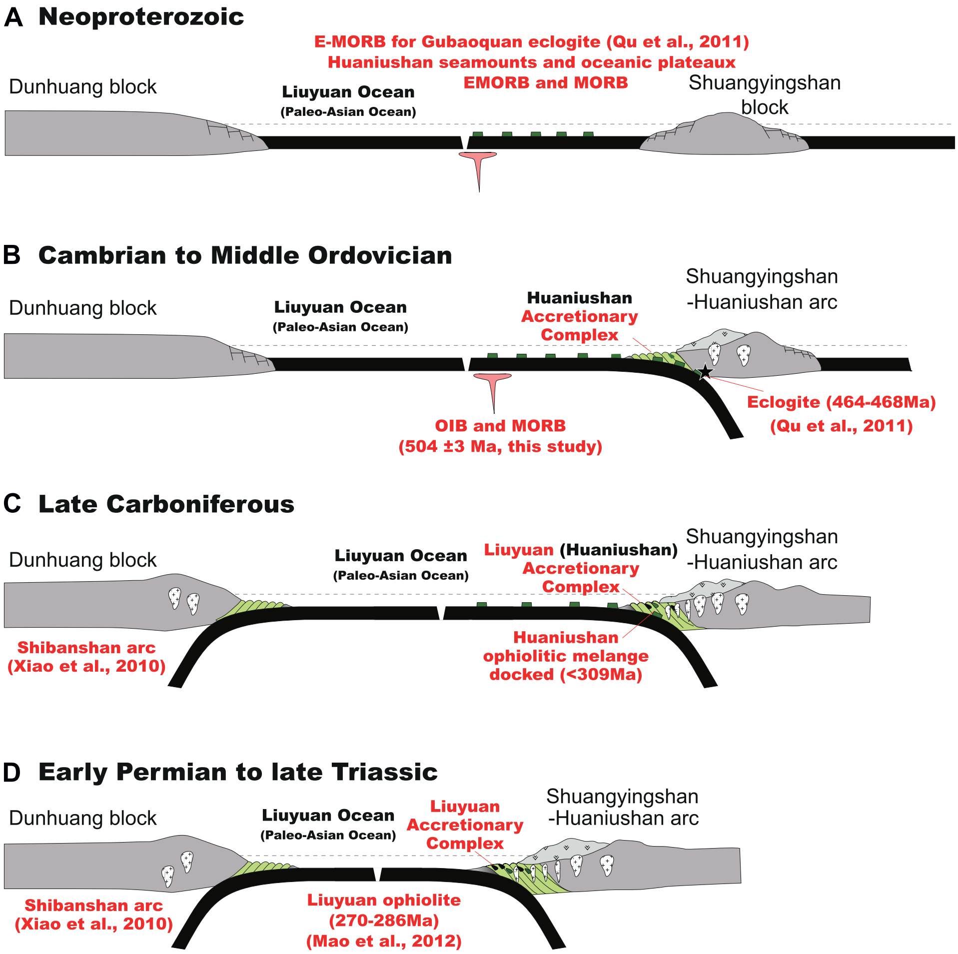

FIGURE 13 | Schematic tectonic diagrams illustrating the development of the Liuyuan accretionary complex in the Beishan orogen, NW China. **(A)** Neoproterozic. **(B)** Cambrian to Middle ordovician. **(C)** Late carboniferous. **(D)** Early permian to late triassic.

Domeier and Torsvik, 2014; Xiao et al., 2018). The compositions and emplaced processes of the Liuyuan accretionary complex are extremely complicated (Zuo et al., 1991; Liu and Wang, 1995; Qu et al., 2011; Mao et al., 2012b; Yu et al., 2012; Zheng et al., 2014; Wang et al., 2016). As discussed above, the oceanic fragments are aged from Neoproterozoic (1,071 Ma) to Middle Permian (270 Ma).

The geochemical and isotopic studies reveal that these ophiolitic mélange blocks have OIB, E-MORB, and MORB geochemical signatures[(Qu et al., 2011; Mao et al., 2012b; Zheng et al., 2014); this study], For example, our studies indicate that the Huaniushan complex consists of OIB, EMORB, and/or MORB fragments; the protolith of the Gubaoquan eclogite is mainly composed of E-MORB and N-MORB fragments (Qu et al., 2011); the Liuyuan ophiolite mainly consists of MORB fragments (Mao et al., 2012b); the fragments of the Yinaoxia ophiolite have an OIB-like mantle source and are metasomatized by fluids and/or melts derived from the subducted slab (Zheng et al., 2014). These data suggest that the oceanic fragments of the Liuyuan accretionary complex are composed of seamounts and the oceanic crust. The 1,071 Ma to 504 Ma E-MORB and OIB fragments indicate that the oceanic island or seamounts is an important component of the Liuyuan oceanic plate. At least, the mantle plume is continuously active from 1,071 Ma to 504 Ma. The clastic sediments and metamorphic clastic blocks of the Liuyuan accretionary complex contain Middle Ordovician to Low strata (GSBGMR, 1989; Wang et al., 2016; Shi et al., 2018; Xu et al., 2019). In summary, the ophiolitic blocks of the Liuyuan accretionary complex consist of Neoproterozoic to Middle Permian seamounts and/or oceanic islands and oceanic crust fragments, Neoproterozoic to Triassic sediments units, and Neoproterozoic to late Triassic granitic and volcanic rocks.

Our data, integrated with published information on the Huaniushan ophiolitic mélange and the Liuyuan accretionary complex in the Beishan orogen, provide new constraints on the tectonic evolution and the geodynamic mechanism of the southern Paleo-Asian Ocean from the late Mesoproterozoic to late Triassic (**Figure 13**):

The Liuyuan ocean, a branch basin of the Paleo-Asian Ocean, may be born in the late Mesoproterozoic (1,071 Ma) by the mantle plume or earlier. Mantle plumes continuously acted from late Mesoproterozoic (1,071 Ma) to late Cambrian (504 Ma) and formed a series of seamounts and/or plateaux (**Figure 13A**). In the late Cambrian to Middle Ordovician (**Figure 13B**), the deep subduction of the seamount with oceanic crust formed the Gubaoquan eclogites (Liu et al., 2011; Qu et al., 2011; Saktura et al., 2017). In the late Carboniferous (**Figure 13C**), the Huaniushan oceanic and seamount ophiolite fragments were docked on the southern margin of the Shuangyinshan–Huaniushan arc. In the early Permian to late Triassic (**Figure 13D**), large volume of the Liuyuan MORB-type ophiolitic blocks suggest that the Liuyuan Ocean was still growing (Mao et al., 2012b; Zheng et al., 2014; Wang et al., 2016), which is consistent with volume of Middle Permian–Triassic arc-related granites formed in the Shibanshan and Huaniushan arc, for example, high-Mg diorite, Nb-enriched dikes, and adakites (Li et al., 2012; Zheng et al., 2020). Finally, this branch of the Paleo-Asian Ocean was closed after 234 Ma (Ao et al., 2021), and the Liuyuan Ocean may have been the final closed branch of the Paleo-Asian Ocean.

CONCLUSION

1. The Huaniushan complex, located in the northernmost part of the Liuyuan accretionary complex, Beishan, is composed of blocks of serpentinized ultramafic rocks, gabbros, basalt, cherts, and limestones within a strongly deformed and cleaved matrix of sandstone and schist.
2. A gabbro block yields zircon U-Pb age of 504 ± 3 Ma. The gabbroic and basaltic blocks have Mid-Ocean-Ridge (MORB)-type and Ocean-Island-Basalt (OIB)-type geochemical characters and high values of $\varepsilon_{Nd}(t)$ (+4.3 to +14.5) and $\varepsilon_{Hf}(t)$ (+8.07 to +17.74).
3. The maximum depositional ages of two sandstone samples (20HNS34 and 20HNS15) from the complex matrix were 309 ± 8 Ma and 501 ± 5 Ma, respectively, indicating that the Huaniushan complex contains matrix rocks varying from 504 Ma to 309 Ma.
4. U-Pb ages and Hf isotopes of detrital zircons from the matrix sandstones indicate that they were derived only from the Shuangyingshan–Huaniushan arc to the north.
5. Available geochronological data reveal that the oceanic blocks and sedimentary matrix of the Liuyuan accretionary complex contain ages of 1,071–270 Ma and 920–234 Ma, respectively. These data suggest that the Liuyuan ocean, a major branch of the Paleo-Asian Ocean may have experienced a prolonged tectonic history, starting in the Late Mesoproterozoic (1,071 Ma), through a long subduction with development of a series of seamounts and/or plateaus emplaced into the Liuyuan accretionary complex in the Paleozoic. The Liuyuan ocean may have been closed later than the late Triassic (234 Ma).

DATA AVAILABILITY STATEMENT

The raw data supporting the conclusion of this article will be made available by the authors, without undue reservation.

AUTHOR CONTRIBUTIONS

All authors have been involved in the study. QM and WX initiated the idea and designed the studies. QM, SA, and MW finished the field, petrology, and geochemical experiments. DS and RL performed the zircon dating and Hf isotopic analysis. HW and ZT processed the geochemical data. QM and SA wrote the original manuscript. WX and BW worked with the geological model and finalized the manuscript.

FUNDING

This study was financially supported by the National Natural Science Foundation of China (41888101, 41822204, and 41802067), the One Hundred Talent Program of the Chinese Academy of Sciences (CAS), the National Key Research and Development Program of China (2017YFC0601201), the Chinese Ministry of Land and Resources for the Public Welfare Industry Research (201411026-1), the “Light of West China” Program of the CAS (2017-XBQNXZ-B-013, 2018-XBYJRC-003), and the Project of China–Pakistan Joint Research Center on Earth Sciences of the CAS (131551KYSB20200021). This is a contribution to IGCP 622.

REFERENCES

Allen, M. B., Engör, A. M. C., and Natal'in, B. A. (1995). Junggar, Turfan and Alakol Basins as Late Permian to ?Early Triassic Extensional Structures in a Sinistral Shear Zone in the Altaid Orogenic Collage, Central Asia. *J. Geol. Soc.* 152, 327–338. doi:10.1144/gsjgs.152.2.0327

Ao, S., Xiao, W., Windley, B. F., Mao, Q., Han, C., Zhang, J. E., et al. (2016). Paleozoic Accretionary Orogenesis in the Eastern Beishan Orogen: Constraints from Zircon U-Pb and 40 Ar/39 Ar Geochronology. *Gondwana Res.* 30, 224–235. doi:10.1016/j.gr.2015.03.004

Ao, S. J., Mao, Q. J., Windley, B. F., Song, D. F., Zhang, Z. Y., and Zhang, J. E. (2021). The Youngest Matrix of 234 Ma of the Kanguer Accretionary Mélange Containing Blocks of N-MORB Basalts: Constraints on the Northward Subduction of the Paleo-Asian Kanguer Ocean in the Eastern Tianshan of the Southern Altaids. *Inter. J. Earth Sci.* 110, 791–808.

Bazhenov, M. L., Collins, A. Q., Degtyarev, K. E., Levashova, N. M., Mikolaichuk, A. V., Pavlov, V. E., et al. (2003). Paleozoic Northward Drift of the North Tien Shan (Central Asia) as Revealed by Ordovician and Carboniferous Paleomagnetism. *Tectonophysics* 366, 113–141. doi:10.1016/s0040-1951(03)00075-1

Boynton, W. V. (1984). “Cosmochemistry of the Rare Earth Elements: Meteorite Studies,” in *Rare Earth Element Geochemistry*. Editor P. Henderson (Amsterdam: Elsevier), 63–114. doi:10.1016/b978-0-444-42148-7.50008-3

Buchan, C., Pfänder, J., Kröner, A., Brewer, T. S., Tomurtogoo, O., Tomurhuu, D., et al. (2002). Timing of Accretion and Collisional Deformation in the Central Asian Orogenic belt: Implications of Granite Geochronology in the Bayankhongor Ophiolite Zone. *Chem. Geol.* 192, 23–45. doi:10.1016/s0009-2541(02)00138-9

Coleman, R. G. (1989). Continental Growth of Northwest China. *Tectonics* 8, 521–635. doi:10.1029/tc008i003p00621

Coutts, D. S., Matthews, W. A., and Hubbard, S. M. (2019). Assessment of Widely Used Methods to Derive Depositional Ages from Detrital Zircon Populations. *Geosci. Front.* 10, 1421–1435. doi:10.1016/j.gsf.2018.11.002

Dobretsov, N. L., Berzin, N. A., and Buslov, M. M. (1995). Opening and Tectonic Evolution of the Paleo-Asian Ocean. *Int. Geol. Rev.* 37, 335–360. doi:10.1080/00206819509465407

Domeier, M., and Torsvik, T. H. (2014). Plate Tectonics in the Late Paleozoic. *Geosci. Front.* 5, 303–350. doi:10.1016/j.gsf.2014.01.002

Duan, J., Xu, G., Qian, Z., Zhang, J., Ma, B., Gao, W., et al. (2021). Petrogenesis and Ni-Cu Exploration Potential of Devonian Mafic–Ultramafic Intrusions in the Southern Part of the Central Asian Orogenic Belt, NW China: Constraints From Zircon O Isotopes and Whole-Rock Sr-Nd Isotopes. *Int. Geol. Rev.* 1–19. doi:10.1080/00206814.2021.1934739

GSBGMR (1989). *Regional Geology of Gansu Province*. Geological Memoirs. Beijing: Geological Publishing House.

Guo, Q., Xiao, W., Hou, Q., Windley, B. F., Han, C., Tian, Z., et al. (2014). Construction of Late Devonian Dundunshan Arc in the Beishan Orogen and its Implication for Tectonics of Southern Central Asian Orogenic Belt. *Lithos* 184-187, 361–378. doi:10.1016/j.lithos.2013.11.007

Hawkins, J. W. (2003). Geology of Supra-subduction Zones-Implications for the Origin of Ophiolites. *Geol. Soc. Am. Spec. Paper* 373, 227–268. doi:10.1130/0-8137-2373-6.227

Hoskin, P. W. O., and Schaltegger, U. (2003). The Composition of Zircon and Igneous and Metamorphic Petrogenesis. *Rev. Mineral. Geochem.* 53, 27–62. doi:10.1515/9781501509322-005

Ji, W. Q., Wu, F. Y., Wang, J. M., Liu, X. C., and Zhang, C. (2020). Early Evolution of Himalayan Orogenic belt and Generation of Middle Eocene Magmatism: Constraint from Haweng Granodiorite Porphyry in the Tethyan Himalaya. *Front. Earth Sci.* 8, 236. doi:10.3389/feart.2020.00236

Kröner, A., Windley, B. F., Badarch, G., Tomurtogoo, O., Hegner, E., Jahn, B. M., et al. (2007). Accretionary Growth and Crust Formation in the Central Asian Orogenic Belt and Comparison with the Arabian-Nubian Shield. *Geol. Soc. Am. Mem.* 200, 181–209. doi:10.1130/2007.1200(11)

Kusky, T. M., Windley, B. F., Safonova, I., Wakita, K., Wakabayashi, J., Polat, A., et al. (2013). Recognition of Ocean Plate Stratigraphy in Accretionary Orogens through Earth History: A Record of 3.8billion Years of Sea Floor Spreading, Subduction, and Accretion. *Gondwana Res.* 24, 501–547. doi:10.1016/j.gr.2013.01.004

Li, S., Wang, T., Tong, Y., Hong, D. W., and Ouyang, Z. Y. (2009). Identification of the Early Devonian Shuangfengshan A-type Granites in Liuyuan Area of Beishan and its Implications to Tectonic Evolution. *Acta Petrol. Mineral.* 28, 407–422. (in Chinese with English abstract)

Li, S., Wang, T., Tong, Y., Wang, Y. B., Hong, D. W., and Ouyang, Z. X. (2011). Zircon U-Pb Age, Origin and its Tectonic Significances of Huitongshan Devonian K-Feldspar Granites from Beishan Orogen, NW China. *Acta Petrol. Sin.* 27, 3055–3070. (in Chinese with English abstract).

Li, S., Wang, T., Wilde, S. A., Tong, Y., Hong, D., and Guo, Q. (2012). Geochronology, Petrogenesis and Tectonic Implications of Triassic Granitoids from Beishan, NW China. *Lithos* 134-135, 123–145. doi:10.1016/j.lithos.2011.12.005

Liu, X. Y., and Wang, Q. (1995). Tectonics of Orogenic Belts in the Beishan Mountains, Western China and Their Evolution. *Geosci. Stud.* 28, 37–48. (in Chinese with English abstract).

Liu, X. C., Wu, G. G., Chen, B. L., and Shu, B. (2002). Metamorphic History of Eclogites from Beishan, Gansu Province. *Acta Geosci. Sin.* 23, 25–29. (in Chinese with English abstract).

Liu, X., Chen, B., Jahn, B. M., Wu, G., and Liu, Y. (2011). Early Paleozoic (Ca. 465 Ma) Eclogites from Beishan (NW China) and Their Bearing on the Tectonic Evolution of the Southern Central Asian Orogenic Belt. *J. Asian Earth Sci.* 42, 715–731. doi:10.1016/j.jseaes.2010.10.017

Liu, Y., Li, W., Ma, Y., Feng, Z., Guan, Q., Li, S., et al. (2021). An Orocline in the Eastern Central Asian Orogenic Belt. *Earth Sci. Rev.* 221, 103808.

Mao, Q., Xiao, W., Fang, T., Wang, J., Han, C., Sun, M., et al. (2012a). Late Ordovician to Early Devonian Adakites and Nb-Enriched Basalts in the Liuyuan Area, Beishan, NW China: Implications for Early Paleozoic Slab-Melting and Crustal Growth in the Southern Altaids. *Gondwana Res.* 22, 534–553. doi:10.1016/j.gr.2011.06.006

Mao, Q., Xiao, W., Windley, B. F., Han, C., Qu, J., Ao, S., et al. (2012b). The Liuyuan Complex in the Beishan, NW China: a Carboniferous-Permian Ophiolitic Fore-Arc Sliver in the Southern Altaids. *Geol. Mag.* 149, 483–506. doi:10.1017/s0016756811000811

Mao, Q., Yu, M., Xiao, W., Windley, B. F., Li, Y., Wei, X., et al. (2018). Skarn-mineralized Porphyry Adakites in the Harlik Arc at Kalatage, E. Tianshan (NW China): Slab Melting in the Devonian-Early Carboniferous in the Southern Central Asian Orogenic Belt. *J. Asian Earth Sci.* 153, 365–378. doi:10.1016/j.jseaes.2017.03.021

Mei, H., Yu, H., Li, Q., Lu, S., Li, H., Zuo, Y., et al. (1998). The First Discovery of Eclogite and Palaeoproterozoic Granitoids in the Beishan Area, Northwestern Gansu Province, China. *Chin. Sci. Bull.* 44, 356–361. (in Chinese).

Mei, H. L., Li, H. M., Lu, S. N., Yu, H. F., Zuo, Y. C., and Li, Q. (1999). The Age and Origin of the Liuyuan Granitoid, Northwestern Gansu. *Acta Petrol. Mineral.* 18, 14–17. (in Chinese with English abstract).

Meschede, M. (1986). A Method of Discriminating between Different Types of Mid-ocean ridge Basalts and continental Tholeiites with the Nb-1bZr-1bY Diagram. *Chem. Geol.* 56, 207–218. doi:10.1016/0009-2541(86)90004-5

Myashiro, A. (1974). Volcanic Series in Island Arc and Active continental Margins. *Am. J. Sci.* 274, 321–355.

Nie, F. J., Jiang, S. H., Bai, D. M., Wang, X. L., Su, X. X., Li, J. C., et al. (2002a). *Metallogenic Studies and Ore Prospectiong in the Conjuction Area of Inner Mongolia Autonomous Region, Gansu Province and Xinjiang Uygur Autonomous Region (Beishan Mt.), Northwest China*. Beijing: Geological Publishing House.

Nie, F. J., Jiang, S. H., Liu, Y., Chen, W., Liu, X. Y., and Zhang, S. H. (2002b). 40Ar/39Ar Isotopic Age Dating on K-Feldspar Separates from Eastern Huanniushan Granite, Gansu Province, and its Geological Significance. *Chin. J. Geology.* 37, 415–422. (in Chinese with English abstract).

Pearce, J. A., Alabaster, T., Shelton, A. W., and Searle, M. P. (1981). The Oman Ophiolite as a Cretaceous Arc-basin Complex: Evidence and Implications. *Philos. Trans. R. Soc. Lond. ser. A* 300, 299–317.

Pearce, J. A. (2008). Geochemical Fingerprinting of Oceanic Basalts with Applications to Ophiolite Classification and the Search for Archean Oceanic Crust. *Lithos* 100, 14–48. doi:10.1016/j.lithos.2007.06.016

Qu, J. F., Xiao, W. J., Windley, B. F., Han, C. M., Mao, Q. G., Ao, S. J., et al. (2011). Ordovician Eclogites from the Chinese Beishan: Implications for the Tectonic Evolution of the Southern Altaids. *J. Metamorp. Geol.* 29, 803–820. doi:10.1111/j.1525-1314.2011.00942.x

Reagan, M. K., Ishizuka, O., Stern, R. J., Kelley, K. A., Ohara, Y., Blichert-Toft, J., et al. (2010). Fore-arc Basalts and Subduction Initiation in the Izu-Bonin-Mariana System. *Geochem. Geophys. Geosys.* 11, Q03X12. doi:10.1029/2009gc002871

Safonova, I. Y., and Santosh, M. (2014). Accretionary Complexes in the Asia-Pacific Region: Tracing Archives of Ocean Plate Stratigraphy and Tracking Mantle Plumes. *Gondwana Res.* 25, 126–158. doi:10.1016/j.gr.2012.10.008

Saktura, W. M., Buckman, S., Nutman, A. P., Belousova, E. A., Yan, Z., and Aitchison, J. C. (2017). Continental Origin of the Gubaoquan Eclogite and Implications for Evolution of the Beishan Orogen, Central Asian Orogenic Belt, NW China. *Lithos* 294-295, 20–38. doi:10.1016/j.lithos.2017.10.004

Schulmann, K., and Paterson, S. (2011). Asian continental Growth. *Nat. Geosci.* 4, 827–829. doi:10.1038/ngeo1339

Şengör, A. M. C., Natal'in, B. A., and Burtman, U. S. (1993). Evolution of the Altaid Tectonic Collage and Paleozoic Crustal Growth in Eurasia. *Nature* 364, 209–304.

Shervais, J. W. (1982). Ti-V Plots and the Petrogenesis of Modern and Ophiolitic Lavas. *Earth Planet. Sci. Lett.* 59, 101–118. doi:10.1016/0012-821x(82)90120-0

Shi, J., Lu, J., Wei, J., Niu, Y., Jiang, T., Han, X., et al. (2018). Petrology, Geochemistry and Sedimentary Environment of Permian Siliceous Rocks in Yingen-Ejin basin and its Adjacent Areas. *Geol. Bull. China* 37, 120–131. (in Chinese with English abstract).

Song, D., Xiao, W., Han, C., Tian, Z., and Wang, Z. (2013). Provenance of Metasedimentary Rocks from the Beishan Orogenic Collage, Southern Altaids: Constraints from Detrital Zircon U-Pb and Hf Isotopic Data. *Gondwana Res.* 24, 1127–1151. doi:10.1016/j.gr.2013.02.002

Song, D., Xiao, W., Windley, B. F., Han, C., and Yang, L. (2016). Metamorphic Complexes in Accretionary Orogens: Insights from the Beishan Collage, Southern Central Asian Orogenic Belt. *Tectonophysics* 688, 135–147. doi:10.1016/j.tecto.2016.09.012

Spencer, C. J., Kirkland, C. L., and Taylor, R. J. M. (2016). Strategies towards Statistically Robust Interpretations of *In Situ* U-Pb Zircon Geochronology. *Geosci. Front.* 7, 581–589. doi:10.1016/j.gsf.2015.11.006

Sun, S. S., and McDonough, W. F. (1989). "Chemical and Isotopic Systematic of Oceanic Basalts: Implicattions for Mantle Composition and Process," in *Magmatism in the Ocean Basins*. Editors A. D. Sauders and M. J. Norry (London, United Kingdom: Geological Society London Special Publication), 3l3–345.

Tian, Z., and Xiao, W. (2020). An Andean-type Arc Transferred into a Japanese-type Arc at Final Closure Stage of the Palaeo-Asian Ocean in the Southernmost of Altaïds. *Geol. J.* 55, 2023–2043. doi:10.1002/gj.3700

Wang, L., Yang, J., Wang, X., Xie, X., Jiang, A., Li, W., et al. (2015). Characteristics of Dashantou Basic-Ultrabasic Complex and its Comprehensive Information Prospecting Model. *Mod. Mining* 2, 72–76. (in Chinese with English abstract).

Wang, Y., Luo, Z., Santosh, M., Wang, S., and Wang, N. (2016). The Liuyuan Volcanic Belt in NW China Revisited: Evidence for Permian Rifting Associated with the Assembly of continental Blocks in the Central Asian Orogenic Belt. *Geol. Mag.* 154, 265–285. doi:10.1017/s0016756815001077

Wilhem, C., Windley, B. F., and Stampfli, G. M. (2012). The Altaids of Central Asia: A Tectonic and Evolutionary Innovative Review. *Earth Sci. Rev.* 113, 303–341. doi:10.1016/j.earscirev.2012.04.001

Winchester, J. A., and Floyd, P. A. (1977). Geochemical Discrimination of Different Magma Series and Their Differentiation Products Using Immobile Elements. *Chem. Geol.* 20, 325–343. doi:10.1016/0009-2541(77)90057-2

Windley, B. F., Alexeiev, D., Xiao, W., Kröner, A., and Badarch, G. (2007). Tectonic Models for Accretion of the Central Asian Orogenic belt. *J. Geol. Soc.* 164, 31–47. doi:10.1144/0016-76492006-022

Wu, F.-Y., Yang, Y.-H., Xie, L.-W., Yang, J.-H., and Xu, P. (2006). Hf Isotopic Compositions of the Standard Zircons and Baddeleyites Used in U-Pb Geochronology. *Chem. Geol.* 234, 105–126. doi:10.1016/j.chemgeo.2006.05.003

Xiao, W. J., Mao, Q. G., Windley, B. F., Han, C. M., Qu, J. F., Zhang, J. E., et al. (2010). Paleozoic Multiple Accretionary and Collisional Processes of the Beishan Orogenic Collage. *Am. J. Sci.* 310, 1553–1594. doi:10.2475/10.2010.12

Xiao, W., Windley, B. F., Allen, M. B., and Han, C. (2013). Paleozoic Multiple Accretionary and Collisional Tectonics of the Chinese Tianshan Orogenic Collage. *Gondwana Res.* 23, 1316–1341. doi:10.1016/j.gr.2012.01.012

Xiao, W., Windley, B. F., Han, C., Liu, W., Wan, B., Zhang, J. E., et al. (2018). Late Paleozoic to Early Triassic Multiple Roll-Back and Oroclinal Bending of the Mongolia Collage in Central Asia. *Earth Sci. Rev.* 186, 94–128. doi:10.1016/j.earscirev.2017.09.020

Xie, J., Di, P., Yang, J., Chen, W., Wei, H., and Zhai, X. (2018). LA-ICP-MS Zircon U-Pb Age, Geochemistry and Tectonic Implications of Metamorphic Dacite from Huanjiushan Group in Beishan Area, Gansu, China. *Northwestern Geol.* 51, 54–64. (in Chinese with English abstract)

Xie, W., Song, X.-Y., Deng, Y.-F., Wang, Y.-S., Ba, D.-H., Zheng, W.-Q., et al. (2012). Geochemistry and Petrogenetic Implications of a Late Devonian Mafic-Ultramafic Intrusion at the Southern Margin of the Central Asian Orogenic Belt. *Lithos* 144-145, 209–230. doi:10.1016/j.lithos.2012.03.010

Xu, W., Xu, X., Niu, Y., Song, B., Chen, G., Shi, J., et al. (2019). Geochronology and Petrogenesis of the Permian marine basalt in the Southern Beishan Region and Their Tectonic Implications. *Acta Geol. Sin.* 93, 1928–1953. (in Chinese with English abstract). doi:10.1111/1755-6724.13758

Yang, J. S., Wu, C. L., Chen, S. Y., Shi, R. D., Zhang, J. X., Meng, F. C., et al. (2006). Neoproterozoic Eclogitic Metamorphic Age of the Beishan Eclogite of Gansu, China: Evidence from SHRIMP U-Pb Isotope Dating. *Geol. China* 33, 317–325. (in Chinese with English abstract).

Yang, J. G., Zhai, J. Y., Yang, H. W., Wang, C. F., Xie, C. L., Wang, X. H., et al. (2010). LA-ICP-MS Zircon U-Pb Dating of basalt and its Geological Significance in Huaniushan Pb-Zn deposit, Beishan Area, Gansu, China. *Geol. Bull. China* 29, 1017–1023. (in Chinese with English abstract).

Yang, Y. H., Zhang, H.-f., Chu, Z.-y., Xie, L.-w., and Wu, F.-y. (2010). Combined Chemical Separation of Lu, Hf, Rb, Sr, Sm and Nd from a Single Rock Digest and Precise and Accurate Isotope Determinations of Lu-Hf, Rb-Sr and Sm-Nd Isotope Systems Using Multi-Collector ICP-MS and TIMS. *Int. J. Mass Spectrom.* 290, 120–126. doi:10.1016/j.ijms.2009.12.011

Yang, J., Wang, L., Xie, X., Qi, Q., Jiang, A., and Zhang, Z. (2016). SHRIMP Zircon U-Pb Age and its Signification of Guaishishan Mafic-Ultramafic Complex in Beishan Mountains, Gansu Province. *Geotecton. Metallog.* 40, 98–108.

Yu, J. Y., Li, X. G., Wang, G. Q., Wu, P., and Yan, Q. J. (2012). Zircon U-Pb Ages of Huitongshan and Zhangfangshan Ophiolite in Beishan of Gansu-Inner Mongolia Border Area and Their Significance. *Geol. Bull. China* 31, 2038–2045. (in Chinese with English abstract).

Zhang, W., Wu, T. R., He, Y. K., Feng, J. C., and Zheng, R. G. (2010). LA-ICP-MS Zircon U–Pb Ages of Xijian Quanzi Alkali-Rich Potassium-High Granites in Beishan, Gansu Province, and Their Tectonic Significances. *Acta Petrol. Mineral.* 29, 719–731. (in Chinese with English abstract).

Zhang, W., Feng, J. C., Zheng, R. G., Wu, T. R., Luo, H. L., He, Y. K., et al. (2011). LA-ICPMS Zircon U–Pb Ages of the Granites from the South of Yin'aoxia and Their Tectonic Significances. *Acta Petrol. Sin.* 27, 1649–1661. (in Chinese with English abstract).

Zhao, Z. H., Guo, Z. J., and Wang, Y. (2007). Geochronology, Geochemical Characteristics and Tectonic Implications of the Granitoids from Liuyuan Area, Beishan, Gansu Province, Northwest China. *Acta Petrol. Sin.* 23, 1847–1860. (in Chinese with English abstract).

Zheng, R., Wu, T., Zhang, W., Meng, Q., and Zhang, Z. (2014). Geochronology and Geochemistry of Late Paleozoic Magmatic Rocks in the Yinwaxia Area, Beishan: Implications for Rift Magmatism in the Southern Central Asian Orogenic Belt. *J. Asian Earth Sci.* 91, 39–55. doi:10.1016/j.jseaes.2014.04.022

Zheng, R. G., Wang, Y. P., Zhang, Z. Y., Zhang, W., Meng, Q. P., and Wu, T. R. (2016). Geochronology and Geochemistry of Yinwaxia Acidic Volcanic Rocks in the Southern Beishan: New Evidence for Permian continental Rift Magmatism. *Geotecton. Metallog.* 40, 1031–1048. (in Chinese with English abstract).

Zheng, R., Li, J., Zhang, J., Xiao, W., and Wang, Q. (2020). Permian Oceanic Slab Subduction in the Southmost of Central Asian Orogenic Belt: Evidence from Adakite and High-Mg Diorite in the Southern Beishan. *Lithos* 358-359, 105406. doi:10.1016/j.lithos.2020.105406

Zindler, A., and Hart, S. (1986). Chemical Geodynamics. *Annu. Rev. Earth Planet. Sci.* 14, 493–571. doi:10.1146/annurev.ea.14.050186.002425

Zuo, G. C., Zhang, S. L., Wang, X., Jin, S. Q., He, G. Q., Zhang, Y., et al. (1990). *Plate Tectonics and Metallogenic Regularities in Beishan Region*. Beijing: Peking University Publishing House.

Zuo, G., Zhang, S., He, G., and Zhang, Y. (1991). Plate Tectonic Characteristics during the Early Paleozoic in Beishan Near the Sino-Mongolian Border Region, China. *Tectonophysics* 188, 385–392. doi:10.1016/0040-1951(91)90466-6

Zuo, G. C., Liu, Y. K., and Liu, C. Y. (2003). Framework and Evolution of the Tectonic Structure in Beishan Area across Gansu Province, Xinjiang Autonomous Region and Inner Mongolia Autonomous Region. *Acta Geol. Gansu* 12, 1–15. (in Chinese with English abstract).

Conflict of Interest: Author QM was employed by the company Redrock Mining CO., Ltd.

The remaining authors declare that the research was conducted in the absence of any commercial or financial relationships that could be construed as a potential conflict of interest.